Geothermics 116 (2024) 102852

Contents lists available at ScienceDirect

Geothermics

journal homepage: www.elsevier.com/locate/geothermics

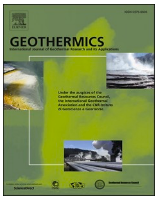

Numerical investigation of closed-loop geothermal systems in deep geothermal reservoirs

Mark White [a,*], Yaroslav Vasyliv [b], Koenraad Beckers [c], Mario Martinez [b], Paolo Balestra [d], Carlo Parisi [d], Chad Augustine [c], Gabriela Bran-Anleu [b], Roland Horne [e], Laura Pauley [f], Giorgia Bettin [b], Theron Marshall [d], Anastasia Bernat [a]

[a] *Pacific Northwest National Laboratory, Richland, WA 99352, USA*
[b] *Sandia National Laboratories, Albuquerque, NM 87155, USA*
[c] *National Renewable Energy Laboratory, Golden, CO 80401, USA*
[d] *Idaho National Laboratory, Idaho Falls, ID 83415, USA*
[e] *Stanford University, Stanford, CA 94305-2004, USA*
[f] *Pennsylvania State University, University Park, PA 16802, USA*

ARTICLE INFO

Keywords:
Closed-loop geothermal
Numerical simulation
Techno-economic analysis
Levelized cost of heat (LCOH)
Levelized cost of electricity (LCOE)
Water working fluid
Supercritical CO_2 working fluid
U-shaped configuration
Coaxial configuration
Porous natural convection
Multi-laterals
Geothermal data repository (GDR)

ABSTRACT

Closed-loop geothermal systems (CLGSs) rely on circulation of a heat transfer fluid in a closed-loop design without penetrating the reservoir to extract subsurface heat and bring it to the surface. We developed and applied numerical models to study u-shaped and coaxial CLGSs in hot-dry-rock over a more comprehensive parameter space than has been studied before, including water and supercritical CO_2 (sCO_2) as working fluids. An economic analysis of each realization was performed to evaluate the levelized cost of heat (LCOH) for direct heating application and levelized cost of electricity (LCOE) for electrical power generation. The results of the parameter study, composed of 2.5 million simulations, combined with a plant and economic model comprise the backbone of a publicly accessible web application that can be used to query, analyze, and plot outlet states, thermal and mechanical power output, and LCOH/LCOE, thereby facilitating feasibility studies led by potential developers, geothermal scientists, or the general public (https://gdr.openei.org/submissions/1473). Our results indicate competitive LCOH can be achieved; however, competitive LCOE cannot be achieved without significant reductions in drilling costs. We also present a site-based case study for multi-lateral systems and discuss how our comprehensive single-lateral analyses can be applied to approximate multi-lateral CLGSs. Looking beyond hot-dry-rock, we detail CLGS studies in permeable wet rock, albeit for a more limited parameter space, indicating that reservoir permeability of greater than 250 mD is necessary to significantly improve CLGS power production, and that reservoir temperatures greater than 200 °C, achieved by going to greater depths (∼3–4 km), may significantly enhance power production.

1. Introduction

Deep (3- to 10-km depths) geothermal resources with temperatures greater than 150 °C are abundant across the continental United States (Blackwell et al., 2011; Tester et al., 2006). These deep heat resources include those with hydrothermal and enhanced geothermal system (EGS) potential. The temperature at depth map (Blackwell et al., 2011) for 6.5 km shows the eastern two-thirds of the continental United States exceeding 100 °C, with considerably hotter regional areas such as the Appalachian trend from Pennsylvania to northern Louisiana, an aquifer-heated region in the Black Hills of South Dakota, and regions along the Gulf Coast of Texas and Louisiana. The map shows temperatures exceeding 225 °C across the Basin and Range Province of the western United States. Hydrothermal systems currently operating in the continental United States are largely concentrated in the Basin and Range Province and along the Pacific Coast in California and require permeability in the deep reservoir rock to actively circulate (i.e., produce and re-inject) water.

EGSs (Brown et al., 2012) overcome the reservoir permeability limitation of hot-dry-rock (HDR) systems by creating permeability via

---

* Corresponding author.
E-mail address: mark.white@pnnl.gov (M. White).

https://doi.org/10.1016/j.geothermics.2023.102852
Received 30 May 2023; Received in revised form 18 October 2023; Accepted 23 October 2023
Available online 3 November 2023
0375-6505/© 2023 Battelle Memorial Institute, Alliance and The Author(s). Published by Elsevier Ltd. This is an open access article under the CC BY-NC-ND license (http://creativecommons.org/licenses/by-nc-nd/4.0/).

fracturing. Closed-loop geothermal systems (CLGSs) are not limited to permeable or impermeable reservoir rock but do benefit from the convective heat transfer present in permeable rock reservoirs. The premise of a CLGS is that the working fluid circulates in a closed loop starting at the ground surface, descending to reservoir depth, potentially traversing the reservoir at depth, and lastly ascending to the ground surface, where its recovered heat is directly utilized (i.e., direct use) or converted to electricity via direct flash or a binary conversion system.

The principal advantage of CLGS over hydrothermal systems is that it eliminates the risks and technological challenges associated with producing and re-injecting water that's in direct contact with the reservoir rock. Risks and challenges include those associated with mineral dissolution, reservoir sustainability, gas release, and potential seismic activity. For EGSs, the risks and challenges are similar due to the direct contact of the working fluid with the reservoir rock, but additionally include fluid lost into the matrix and natural fractures that are unconnected to the injection and/or production boreholes. Although the rock matrix of an EGS reservoir is generally considered impermeable, the high pressures of EGSs yield fluid leak-off over time.

The ability to numerically predict the thermal performance of geothermal systems, whether they're hydrothermal, EGS, or CLGS, has proven invaluable for making informed decisions about the economic viability of proposed systems, and considerable effort has gone into developing analytical, semi-analytical, and detailed numerical simulation approaches. One of the foundational papers with respect to CLGSs is that of Ramey (1962), who was concerned with modeling heat exchange between a working fluid and matrix rock for a petroleum industry application. Ramey developed an algebraic equation for determining the temperature of a fluid flowing in a wellbore as it loses (or gains) heat to (from) the geologic formation via heat conduction. This model can be adapted for analyzing u-shaped CLGSs by applying it in sequence to the descending, horizontal, and insulated ascending sections of the CLGS. Horne (1980) also developed a foundational semi-analytical model for computing the thermal performance of CLGSs with a coaxial (tube-in-tube) configuration. The model allows for downward flow in either the center tube or annulus and assumes radial heat conduction in the surrounding formation. A synopsis of these foundational studies is provided in Appendix A: Foundational Studies.

For more general analysis, including deviated wells, alternative working fluids (e.g., supercritical CO_2 (sCO_2)), multi-lateral CLGS, and porous natural convection, more general numerical models have been developed. Morita led the development and application of a finite-difference-based numerical simulator for modeling the thermal performance of a vertical coaxial configuration (Morita et al., 1984; Morita and Matsubayashi, 1986, Morita et al., 1992a), which showed excellent agreement with a short field experiment in Hawaii (Morita et al., 1992b). Schulz (2008) developed and applied a numerical simulator and coupled economic analysis module to investigate the thermal performance, electricity generating potential, and achievable incomes.

More recently, a series of researchers have developed numerical simulators for alternative working fluids. Oldenburg et al. (2016) completed an early investigation of using sCO_2 as the working fluid in a u-shaped configuration using the TOUGH simulator (Pruess et al., 2012) with its T2Well model (Pan et al., 2011, 2014). Sun et al. (2018) also developed a numerical simulator for sCO_2 and explored the impact of mass flow rate and inlet pressure. Song et al. (2018a, b) developed a numerical simulator for u-shaped and coaxial CLGS, both with water as the working fluid. These studies considered variations in mass flow rate, inlet temperature, horizontal extent, and wellbore diameter. Zhang et al. (2021) developed a finite-difference-based numerical simulation model to compare thermal performance differences between u-shaped and coaxial configurations, also with water as the working fluid, but limited to a 1-year operational period. Wang et al. (2020) and Beckers et al. (2022) presented models for single- and multi-lateral CLGS. Beckers et al. (2022) include an economic model to compare the costs of different configurations and working fluids.

A recent review of technical papers on CLGS revealed an exponential growth in publications from 2001 through 2021 (Budiono et al., 2022), highlighting the interest in these systems. However, as pointed out by Budiono et al. (2022), the extent of independent parameters considered in these studies was limited and the results were not easily accessible to the public. Given the renewed recent interest in CLGS, the present study was funded by the Geothermal Technologies Office within the U.S. Department of Energy (DOE) Office of Energy Efficiency and Renewable Energy as a collaborative working effort to use numerical simulation to better characterize the potential and limitations of CLGSs from a techno-economic perspective. In this paper, we present the results of this study, including the numerical models developed to simulate u-shaped and coaxial CLGSs in HDR (heat transfer via thermal conduction from the geothermal reservoir) over a more comprehensive parameter space than has been considered before, including water and sCO_2 as working fluids. Moreover, an economic analysis of each realization was developed to evaluate the levelized cost of heat (LCOH) for direct heating application and levelized cost of electricity (LCOE) for electrical power generation. We also present results for multi-lateral systems and for CLGS in permeable formations, the latter showing significant performance enhancement via buoyantly driven convection currents.

2. Subsurface numerical models and validation studies

This study was aimed at providing simulation results across two heat-exchanger configurations: u-shaped and coaxial (Fig. 1); two working fluids: water and sCO_2; and seven simulation parameters: mass flow rate, depth, horizontal extent, geothermal gradient, borehole diameter, inlet temperature, and rock thermal conductivity, as applied to either a direct-use or power production scenario. The working group used a wide array of computing capabilities to model the heat recovery of these two heat exchangers (as well as multi-lateral variants) emplaced in deep geothermal reservoirs characterized as either HDR or hot-wet-rock.

Each of the national laboratories involved in the study had internally developed computational capabilities that could be used in modeling the heat recovery from deep geothermal reservoirs using CLGS configurations. The Idaho National Laboratory (INL) geothermal software suite is composed of three parts: 1) a Python language-based codes-coupling interface (Parisi et al., 2023); 2) the RELAP5-3D system thermal-hydraulic code, RELAP5-3D (RELAP5-3D Code Development Team, 2018a, b); and 3) the MOOSE platform-based (Gaston et al., 2015) FALCON code, a finite-element thermal-hydraulic-mechanical-chemical code (Podgorney et al., 2021). The two codes were coupled via a Python script with FALCON receiving heat flux and fluid temperature from RELAP5-3D and RELAP5-3D receiving wall temperatures from FALCON. The HDR model, developed by the National Renewable Energy Laboratory (NREL), is applicable to incompressible and compressible working fluids and is based on the Beckers et al. (2015) slender-body theory (SBT) model, recently improved by Beckers et al. (2022). The SBT model uses an analytic Green's function to model the heat conduction in the formation, use of an enthalpy formulation for the 1D area-averaged fluid energy equation, and allowing to simulate multiple, curved, thermally interacting heat exchangers, such as a multi-lateral u-loop configuration. Pacific Northwest National Laboratory (PNNL) applied the STOMP-GT (Subsurface Transport Over Multiple Phases Simulator—Geothermal) reservoir simulator with its embedded fracture and borehole modeling capabilities (White and Fu, 2020). This modeling approach couples a conventional finite-volume based solution of multi-phase fluid flow and heat transport in the rock matrix with a borehole via a piecewise Peaceman well index (White et al., 2013). Within the borehole, the Gnielinski correlation (Gnielinski, 1975; Incropera and DeWitt, 2007) for turbulent flow is used to calculate the Nusselt number for heat transfer between the working fluid and borehole wall, with the wall shear stress modeled using the Darcy-Weisbach friction factor formulation (Incropera and DeWitt, 2007), where the non-dimensional wall shear stress i.e., the friction

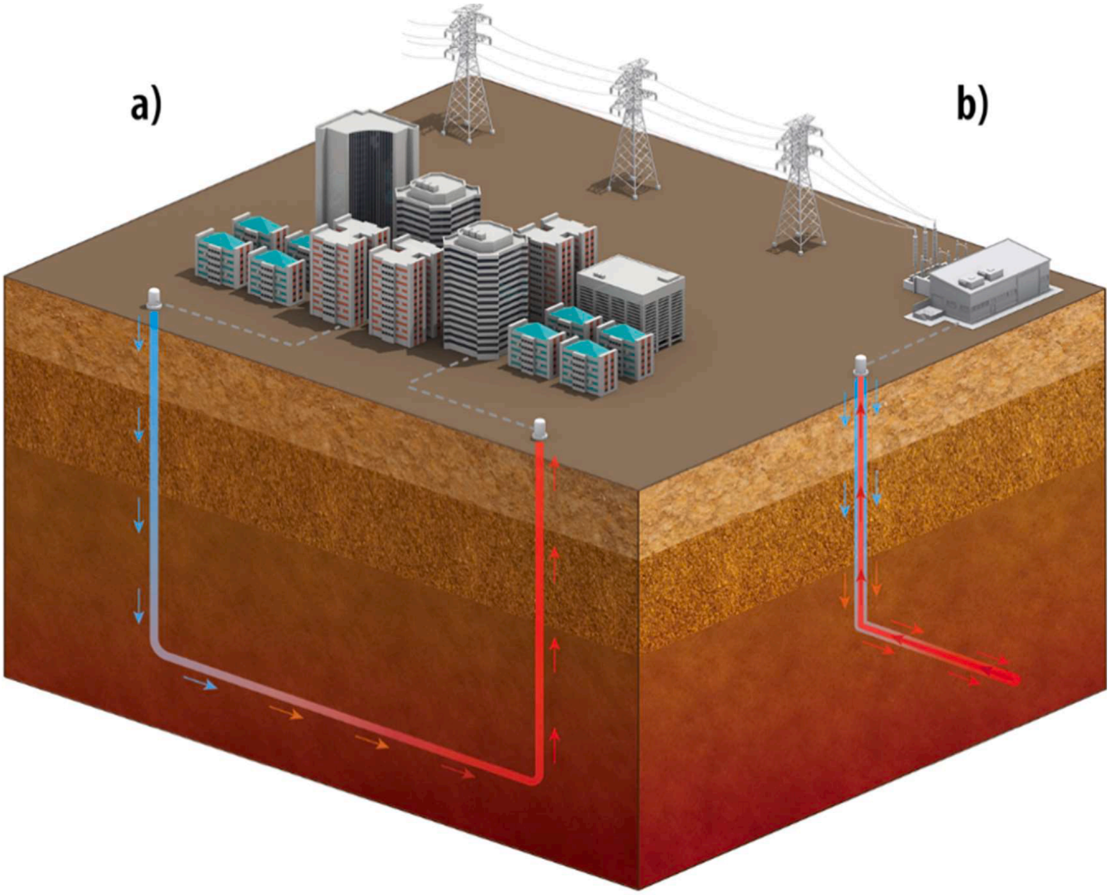

Fig. 1. Two common types of closed-loop geothermal systems are (a) u-shaped design (with one or multiple laterals) and (b) coaxial design or "pipe-in-pipe" configuration. Image credit: NREL.

factor, is obtained through the explicit Haaland fitting (Munson et al., 2013).

Sandia National Laboratories (Sandia) applied the multi-physics code Sierra (Sierra Thermal Fluid Development Team, 2020), with coupled simulation capabilities for thermal, fluid, aerodynamics, solid mechanics, and structural dynamics. Sandia's models (Beckers et al., 2023; Vasyliv et al., 2021) were developed using the thermal-fluids code Aria (Sierra Thermal Fluid Development Team, 2020). Their borehole fluid model, applicable to incompressible (e.g., liquid water) and compressible fluids (e.g., sCO_2), consists of a 1D steady state momentum equation coupled to a 1D area-averaged thermal energy equation with fluid properties tabulated using CoolProps (Bell et al., 2014). For the momentum equation, inertial, pressure, viscous, and gravitation forces are included, with viscous forces modeled using a non-dimensional wall shear stress formulation. For the fluid thermal energy equation, source terms are included to account for the thermal expansion of the circulating fluid as well as irreversible heating due to viscous dissipation. Depending on whether the formation is permeable (hot-wet-rock) or not (HDR), heat exchange is included by coupling the 1D area-averaged thermal energy equation to either a 2D axisymmetric transient heat conduction domain or a 3D porous domain, through a convective flux boundary condition. Sandia's HDR model employed two configurations, one for u-shaped heat exchangers (Fig. 2(a)) and a second for coaxial heat exchangers (Fig. 2(b)). In both models, adiabatic boundary conditions are applied to the remaining formation boundaries and the formation outer radius is set to 150 m. This formation radius was sufficient to enclose the thermal drawdown from energy extraction at the borehole.

2.1. *Utah FORGE site with water working fluid*

Comparisons were made across the national laboratory simulators against analytical solutions and against Morita's 1992 field experiments (Parisi et al., 2021; Vasyliv et al., 2021; White et al., 2021), indicating general good agreement between all codes. Here, we highlight two results: a u-shaped heat-exchanger circulating water as a working fluid and a coaxial heat-exchanger circulating sCO_2. Fig. 3 presents outlet temperature versus time for a u-shaped heat exchanger hypothetically installed at the Utah FORGE site, located near active hydrothermal resources in the southeast margin of the Great Basin near Milford, Utah. Utah FORGE is a DOE-funded initiative for research and development of EGSs. Temperatures at the lowest depth are about 200 °C and follow a nonlinear gradient (Podgorney et al., 2020).

Two u-shaped systems were used for the intercomparison of simulation results, which resulted from system optimizations based on thermal and mechanical objective functions (White et al., 2021). In both problems, the geothermal gradient was 0.0788 °C/m (78.8 °C/km), depth was 2.539 km (i.e., bottom-depth temperature of 225 °C), horizontal extent was 10.0 km, thermal conductivity was 3.05 W/m K, specific heat capacity was 790 J/kg K, and density was 2750 kg/m^3. The first problem used a mass flow rate of 11.8 kg/s, with insulation installed in the ascending section over the upper 1.174 km, and the second problem used a mass flow rate of 38 kg/s with insulation installed in the upper 0.875 km. As shown in Fig. 3, results from Sandia, PNNL, Stanford solution (Horne and Shinohara, 1979), and NREL's Hagoort (2005) semi-analytical solution showed close agreement between outlet temperatures and time.

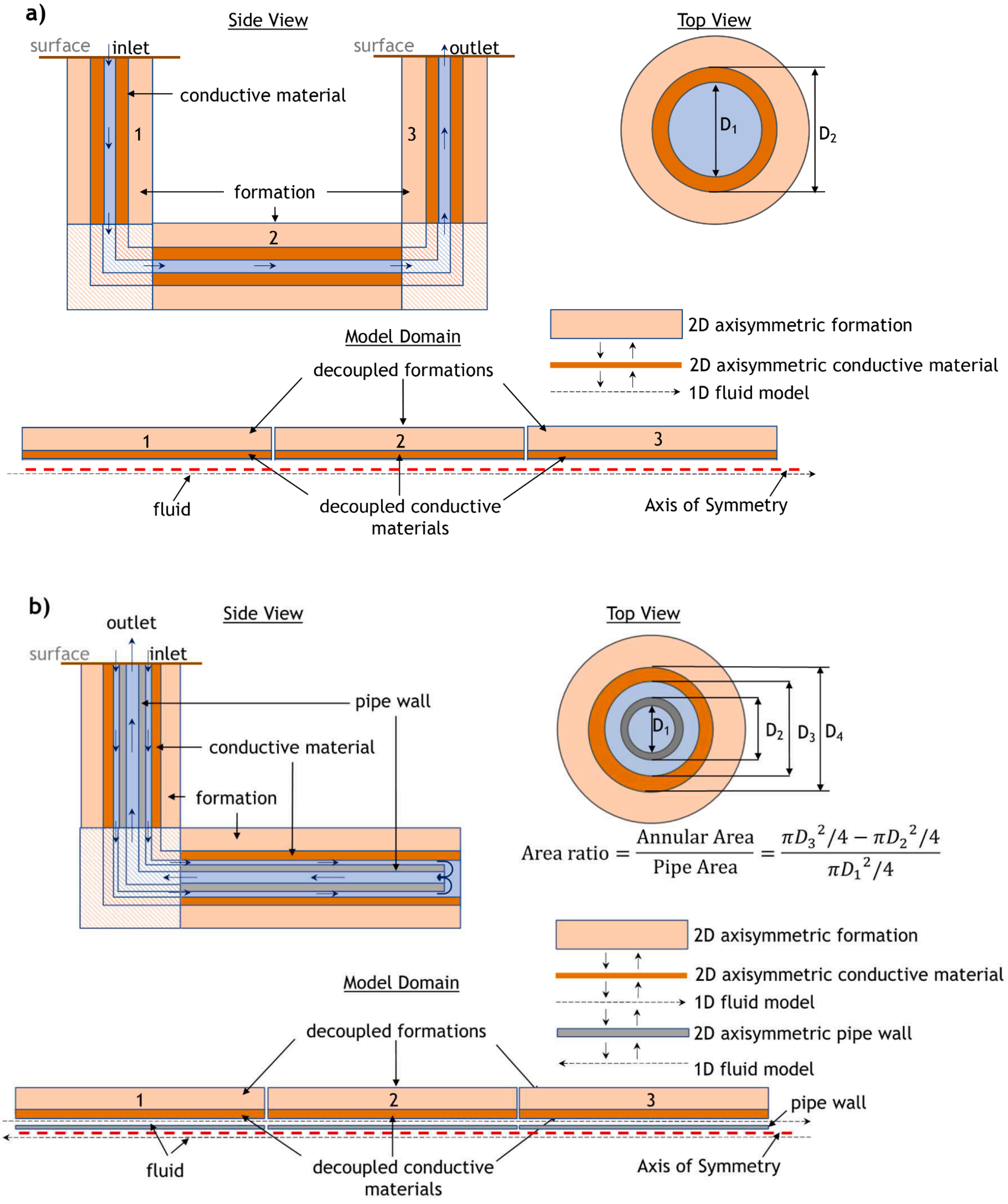
a)
Side View
surface
inlet
surface
outlet
conductive material
1
3
formation
2
Top View
D1
D2
Model Domain
decoupled formations
2D axisymmetric formation
2D axisymmetric conductive material
1D fluid model
1
2
3
fluid
decoupled conductive materials
Axis of Symmetry
b)
Side View
outlet
surface
inlet
pipe wall
conductive material
formation
Top View
D1
D2
D3
D4
Area ratio = Annular Area / Pipe Area = $\pi D_3^2/4 - \pi D_2^2/4$ / $\pi D_1^2/4$
Model Domain
decoupled formations
2D axisymmetric formation
2D axisymmetric conductive material
1D fluid model
2D axisymmetric pipe wall
1D fluid model
1
2
3
pipe wall
fluid
decoupled conductive materials
Axis of Symmetry

Fig. 2. Sandia National Laboratories 2D axisymmetric model for the (a) u-shaped configurations and (b) coaxial configurations in hot-dry-rock (HDR). The mesh (not shown) is biased toward the borehole to resolve the radial temperature gradients. The HDR formations labeled 1, 2, and 3 are decoupled from each other, except through heat exchange with the circulating fluid. An optional enhanced conductive zone is shown.

2.2. *Sandia and NREL comparison study with sCO_2 working fluid*

As an additional verification, the Sandia model (Beckers et al., 2023) was validated against the SBT model (Beckers et al., 2015) for both water and sCO_2 as well as for both heat exchanger designs. Fig. 4 highlights results for Case 11 reported in Beckers et al. (2022), where sCO_2 is injected down the annulus of a coaxial heat exchanger at 20 kg/s, 40 °C, and 10 MPa (100 bar), with a 2-km bottom borehole temperature of 200 °C. Here, the test case has been modified to include a 6-km lateral extension. As can be seen, the numerical solutions of both models show excellent agreement with each other, with the outlet temperatures indistinguishable from each other. Other cases investigated showed similar agreement.

3. Techno-economics of CLGS in hot-dry-rock

The execution speed of the Sandia HDR modeling approach and their verified accuracy on problems involving both u-shaped and coaxial configurations circulating either water or sCO_2 as working fluids, as noted above, opened the way to investigating HDR CLGSs across a larger parameter space than has been previously done. The following two sections detail the below-ground database of HDR numerical solutions

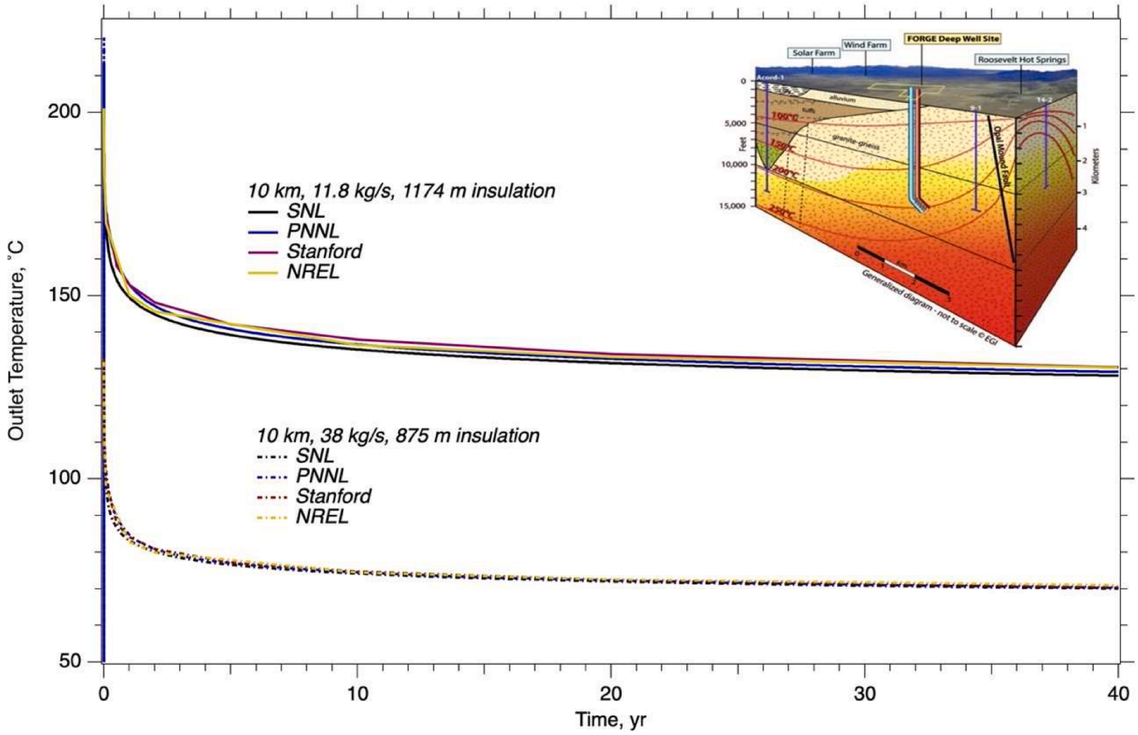

Fig. 3. Comparison of HDR outlet temperature versus time for two Utah FORGE-based scenarios for the various numerical models, where SNL is SNL's 2D axisymmetric model, PNNL is STOMP-GT, Stanford is the Horne and Shinohara (1979) analytical solution, and NREL is the Hagoort (2005) semi-analytical solution. Inset image provides an overview of the FORGE site geologic and thermal setting.

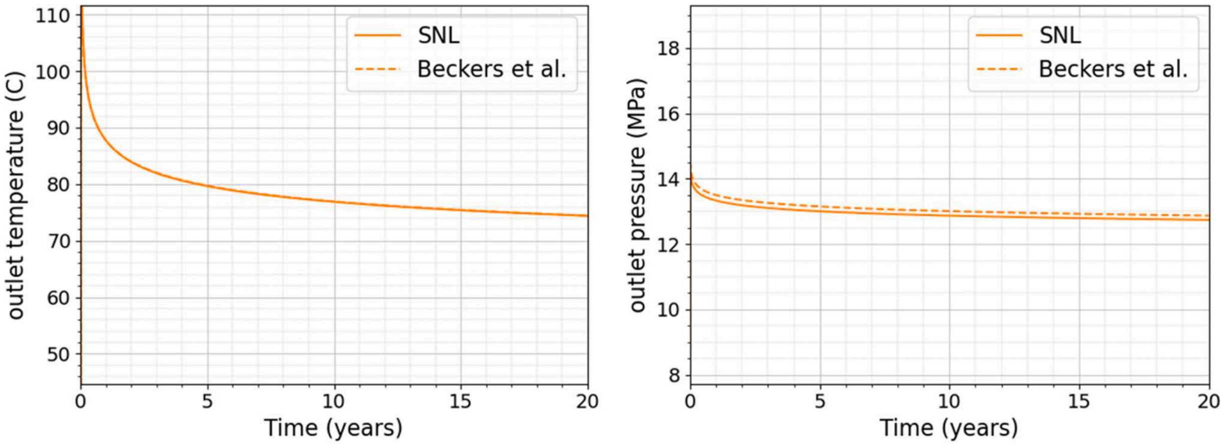

Fig. 4. Outlet temperature (left) and outlet pressure (right) for a coaxial heat exchanger with sCO_2 fluid flowing down the annulus. The Sandia model ("SNL," solid line) and Beckers et al. SBT model (dotted line) show excellent agreement. These results correspond to a 6-km lateral extension of Case 11 as detailed in Beckers et al. (2022).

tabulated using Sandia's model and NREL's above-ground plant and economic model. To lower the entry barrier for potential users, the below-ground and above-ground results were combined into a single Python-based web application, *GeoCLUSTER*, hosted on the Geothermal Data Repository at https://gdr.openei.org/submissions/1473. *GeoCLUSTER* provides a graphical user interface to explore and visualize both the dataset and the above-ground techno-economic results (e.g., LCOE/LCOH). Its primary target audience are those looking to make preliminary assessments of system performance and economic outcomes of proposed installations. Additional details regarding the database can be found in Beckers et al. (2023) and are described below.

3.1. *Below-ground HDF5 database*

The HDF5 database maps simulation inputs (i.e., parameter space) to measured responses (i.e., outlet temperature and pressure versus time). In creating the parameter space, we considered two working fluids (i.e., water and sCO_2) and two heat exchanger designs (coaxial and u-shaped). Each heat exchanger and working fluid combination was evaluated for up to 40 years at the Cartesian product of seven independent parameters (mass flow rate, horizontal extent, vertical drilling depth, rock geothermal gradient, borehole diameter, injection temperature, and rock thermal conductivity) discretized using equally spaced points as listed in Table 1. This choice of discretization is by no means optimal as it suffers from the curse of dimensionality. As a result, certain input

Table 1

Variable and fixed CLGS parameters. Here, k is thermal conductivity, α is thermal diffusivity, and $\frac{k}{\sqrt{\alpha}}$ is a thermal characteristic of geothermal rock reported in Nalla et al., 2005.

Variable parameters				Fixed parameters		
Description	Bounds	Units	Count	Description	Value	Units
Mass flow rate	5 to 100	kg/s	26	Inlet pressure	20.0	MPa
Horizontal extent	1000 to 20,000	m	20	Ambient temperature	26.85	°C
Vertical depth	1000 to 5000	m	9	Surface temperature	25.0	°C
Geothermal gradient	0.03 to 0.07	°C/m	5	Pipe roughness	0.025	mm
Borehole diameter	0.2159 to 0.4445	m	3	Rock density	2750	kg/m^3
Inlet temperature	30 to 60	°C	3	Rock specific heat	790	J/kg K
Rock thermal conductivity	1.5 to 4.5	W/m K	3	Inner pipe/annulus area ratio	1.0	
Rock $\frac{k}{\sqrt{\alpha}}$	1805 to 3127	J/m^2 s$^{1/2}$ K		Inner pipe thickness	0.0192	m
				Inner pipe thermal conductivity	0.06	W/m K

dimensions may not be adequately resolved. This is especially prominent when one of the dependent variables (e.g., outlet pressure) exhibits a strong nonlinearity (e.g., with respect to hydraulic diameter). In this scenario, if the query point is far away from a known solution, the interpolation error can be large. No attempt is made to provide error bounds, and users of the database should keep these limitations in mind.

The parameters in Table 1 are intended to cover a wide range of conventional and hypothetical scenarios. Nalla et al. (2005) noted that the pseudo-steady-state (i.e., post early transient) outlet temperature of coaxial CLGSs was dependent on the thermal characteristic parameter $\frac{k}{\sqrt{\alpha}}$, where k is the thermal conductivity and a is the thermal diffusivity. Nalla et al. (2005) considered a range of $\frac{k}{\sqrt{\alpha}}$ parameters for sedimentary and evaporite formations (spanning values from 173 to 1881 J/m^2 s$^{1/2}$ K). Our range for the parameter $\frac{k}{\sqrt{\alpha}}$ includes the value of 2353 J/m^2 s$^{1/2}$ K reported for The Geysers, California (Barker et al., 1991), the average value of 2700 J/m^2 s$^{1/2}$ K for granitic rock within our temperature range (Heuze, 1983), and an upper bound value near the 3200 J/m^2 s$^{1/2}$ K reported for granites with 50 % quartz (Robertson, 1988). Horizontal extents in Table 1 are probably beyond those of current drilling capabilities but represent total lengths that might be achievable via multiple laterals. Lastly, depth and geothermal gradient ranges in Table 1 were chosen such that the bottom borehole temperature is below the critical temperature of water (374 °C).

Across the considered heat exchanger configurations and working fluid combinations, our discretization results in over 2.5 million simulations. These simulations were executed in batches of concurrent runs using the Sandia Dakota package (Adams et al., 2021). The results were stored in a single HDF5 file and compressed using a low-rank singular value decomposition. Specifically, for each heat exchanger-working fluid combination, only the singular values and left and right singular vectors are stored for the corresponding temperature and pressure outlet states as described in Beckers et al. (2023). Since the normalized singular values quickly drop off, we found storing a rank 4 or 5 decomposition results in less than 0.5 % relative error across any simulation or point in time. In this manner, large compression ratios were obtained due to similarities across the solution space.

In addition to storing the outlet states, the produced heat and available work were computed and stored. Produced heat, W_t, is computed from the enthalpy difference between the injected and produced fluid:

$$W_t = \int_{t=0}^{t=T} \dot{m}\ \Delta h\ dt$$

where $\dot{m}$ is mass flow rate, Δh is the difference between outlet- and inlet-specific enthalpy, and t is time. Available work, W_e, is computed from the difference in exergy between injected and produced fluid:

$$W_e = \int_{t=0}^{t=T} \dot{m}\ (\Delta h - T_{amb}\ \Delta s)\ dt$$

where W_e is available work, T_{amb} is ambient temperature (K), and Δs is difference between outlet- and inlet-specific entropy. This available work is agnostic to the above-ground energy conversion configuration and represents the maximum amount of electricity (or useful work) that can be theoretically extracted based on the second law of thermodynamics. Actual electricity generation, addressed later in this article, depends on the energy conversion system employed and is significantly less than the theoretical maximum for temperatures encountered in geothermal systems.

Table 2

Geologic and system design parameters for example u-shaped CLGS. Rock-specific heat capacity, density, and other fixed parameters are listed in Table 1.

Horizontal extent	Depth	Geothermal gradient	Borehole diameter
10 km	2.5 km (bgs)	0.065 °C	0.3 m
Inlet temperature	Thermal conductivity	Reservoir temperature	Configuration
40 °C	3.5 W/m K	187.5 °C	u-shaped

3.2. Above-ground plant and economic model

To address the economic aspects of CLGSs, net averaged present costs are computed using the "standard discounting model" from GEOPHIRES (Beckers and McCabe, 2019). Specifically, the LCOH and LCOE are computed as:

$$LCOH = \frac{sum\ of\ costs\ over\ lifetime}{sum\ of\ heat\ produced} = \frac{\sum_{t=1}^{n} \frac{C_t+O_t}{(1+r)^t}}{\sum_{t=1}^{n} \frac{E_h}{(1+r)^t}}$$

$$LCOE = \frac{sum\ of\ costs\ over\ lifetime}{sum\ of\ electricity\ generated} = \frac{\sum_{t=1}^{n} \frac{C_t+O_t}{(1+r)^t}}{\sum_{t=1}^{n} \frac{E_e}{(1+r)^t}}$$

where C_t is capital expenditures (CAPEX) in year t, O_t is operating and maintenance expenditures in year t, n is the expected lifetime of the CLGS, r is the discount rate, E_h is the heat produced in year t, and $E_e$is the electricity generated in year t.

For water as the heat transfer fluid, an organic Rankine cycle (ORC) was assumed with efficiency correlations for conversion from heat to electricity based on the thermal efficiency correlations developed by Augustine (2009) and utilization efficiency correlations (based on produced exergy) developed by Beckers (2016) and implemented in GEOPHIRES (Beckers and McCabe, 2019). For sCO$_2$ as the circulating fluid, we assumed a steady-state direct turbine expansion cycle where the circulating sCO$_2$ is also the working fluid through the cycle. We implemented the approach of Wang et al. (2022), where, after turbine expansion, the CO_2 is cooled ("pre-cooling"), followed by compression, and then cooled again ("post-cooling") to injection conditions. CO_2 temperature and pressure at each step in the cycle are either calculated or user specified. CoolProp (Bell et al., 2014) tables are used to obtain values for properties such as enthalpy and entropy. Turbine power generation and compressor power consumption are based on a user-provided isentropic efficiency. Pre-cooling and post-cooling assume direct air cooling with fans. Fan power consumption is calculated based on required air flow rate and assuming 0.25 kW_e per kg/s of required air (Augustine, 2009).

Simple cost correlations are implemented to calculate capital and operation and maintenance (O&M) costs. Drilling costs and surface plant costs are considered to estimate overall system capital cost. Drilling costs are calculated by multiplying the total drilling depth by a drilling cost per meter, with \$1000/m as the default value. Existing well drilling cost correlations (e.g., Lowry et al., 2017) are not implemented because closed-loop well design may be different (e.g., long open-hole laterals) and total well drilling measured depth may be beyond typical drilling depths (Beckers and Johnston, 2022). For reference baseline drilling costs from Lowry et al. (2017) across small and large diameters, vertical open boreholes, and horizontal lined boreholes, ranged from \$1410/m to \$3567/m. Surface plant costs are based on the size of the plant, with plant-specific cost values based on findings by Beckers and Johnston (2022), Beckers et al. (2022), and Beckers and McCabe (2019). For electricity generation, a default value of \$3000/kW_e is assumed. For direct-use heat, the surface plant cost assumes a default value of \$100/kW_{th} – this represents costs for the heat exchanger, piping, and valves but not a district heating system. The O&M cost is calculated as a percentage of the surface plant investment cost with 1.5 % as default value, based on research by Beckers and Johnston (2022). Because the fluid circulates in a closed loop, no scaling or corrosion issues are anticipated, and no wellfield maintenance costs are considered. For direct use, pumping costs are accounted for by considering a user-provided electricity rate. For electricity as end-use, the pumping power is subtracted from the plant electricity output. Many closed-loop designs, however, are characterized by a strong thermosiphon effect and do not require pumping power. Capital or O&M costs for potential exploration, well redrilling, well field maintenance, and land leasing are not considered.

3.3. Limitations of CLGS in hot-dry-rock

Before detailing LCOEs and LCOHs for the heat exchangers and working fluids being considered, it is important to comment on the limitations of CLGSs in HDR. Early studies by Ramey (1962) for u-shaped configurations and Horne (1980) for coaxial configurations, and later studies by Nalla et al. (2005) and Oldenburg et al. (2016) for sCO_2, demonstrated that production temperatures in HDR reservoirs decay over time to much lower temperatures than are imposed at the outer radial rock by the thermal gradient.

The root cause of the temperature decay is that as the circulating fluid advects away the thermal energy of the adjacent hot rock, heat conduction (the sole heat transfer mechanism) simply cannot transfer thermal energy from the outer radial extents to the depleted rock core surrounding the borehole at a sufficient rate. As a result, the CLGS production temperatures decay over time and thermal output and available power drop accordingly. Figs. 5 and 6 show examples of the thermal output and available power profiles, respectively, as a function of time adhering to this prototypical behavior of CLGS solutions in HDR. Here, a conventional u-shaped CLGS is circulating either water or sCO_2 at three mass flow rates (25, 50, and 100 kg/s) for up to 40 years. Geologic and system design parameters are listed in Table 2.

As with EGS, the primary mechanism to overcome these limitations of heat conduction would be to significantly increase the heat transfer surface area. In the context of the CLGSs in HDR, the only reasonable mechanisms to do this are either to extend the borehole and or increase its diameter, both of which would normally increase capital cost. In fact, as discussed next, even extending to 30 km of total drilling with a maximum depth of 5 km is insufficient to economically convert the

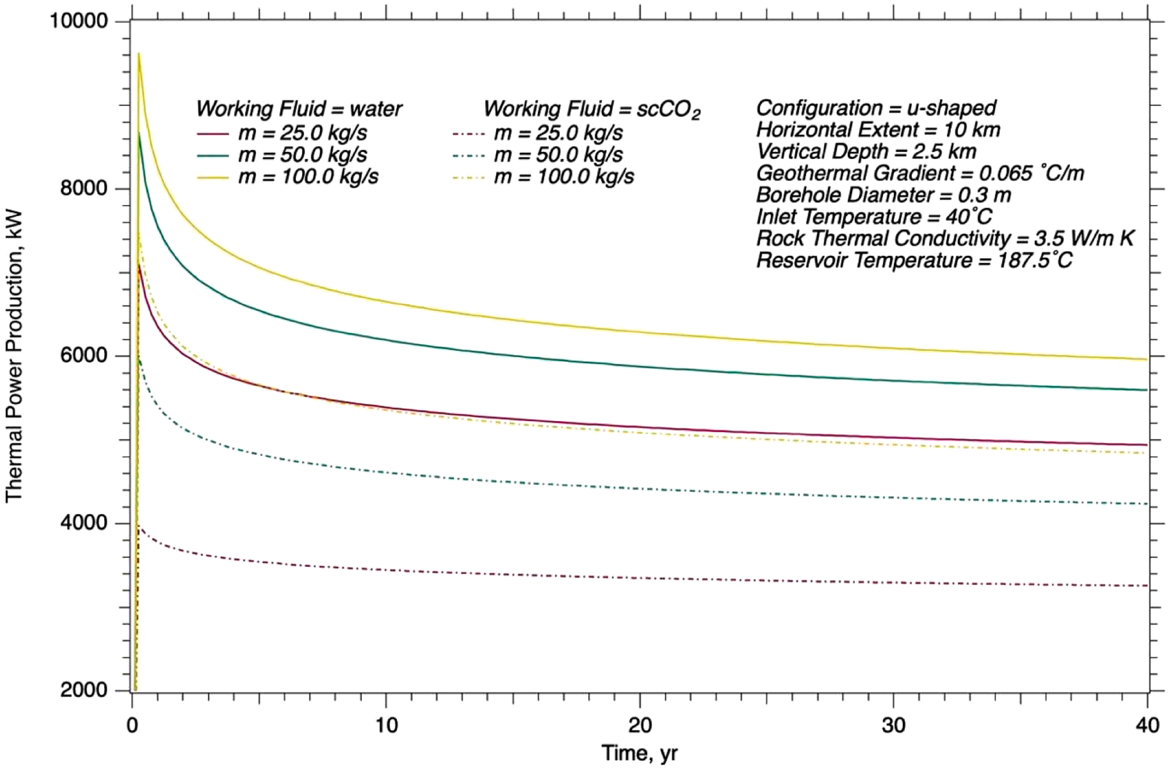

Fig. 5. Thermal power $m\Delta h$ versus time for a conventional u-shaped CLGS as a function of mass flow rate and working fluid.

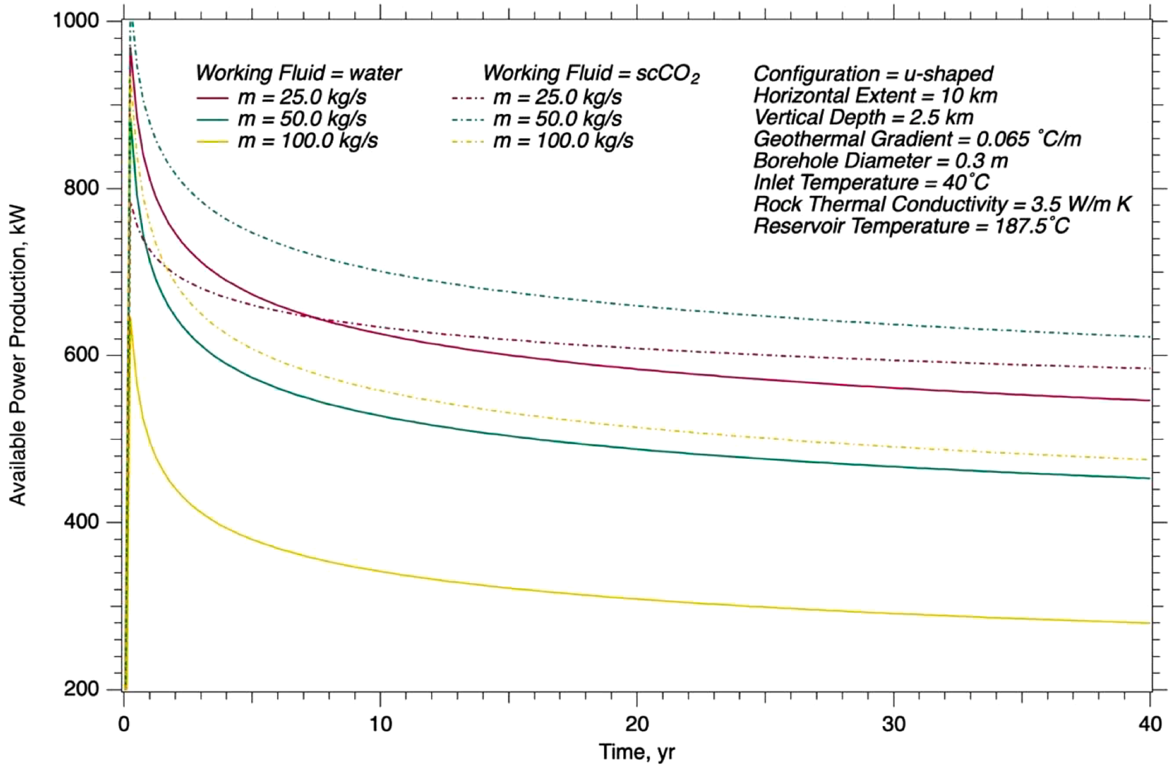

Fig. 6. Available power $m(\Delta h - T_{amb}\Delta s)$ versus time for a conventional u-shaped CLGS as a function of mass flow rate and working fluid.

thermal output to electrical power unless significant drilling cost reductions are assumed. This is despite considering a HDR reservoir that is well into the upper end of the geothermal resource base and despite considering total drilling lengths well beyond what has been demonstrated in the field.

3.3.1. LCOE for single-lateral designs

U.S. Secretary Jennifer M. Granholm recently announced a new DOE goal to make EGS a widespread renewable energy option in the U.S. by targeting an LCOE of $45/MWh$_e$ by 2035 (DOE, 2022). Using the default economics values in the *GeoCLUSTER* web application, we can determine if CLGS in HDR can meet this target. For this example, maximum values from Table 1 for depth, geothermal gradient, rock thermal conductivity, and borehole diameter were used (i.e., 30-km total borehole length, 0.4445-m (17.5-in.) borehole diameter, 375 °C bottom borehole temp, and $\frac{k}{\sqrt{\alpha}} = 3127$ J/m^2 s$^{1/2}$ K). Table 3 summarizes the optimal mass flow rate, average heat production, average electricity generation, outlet temperature, and outlet pressure for the different designs that correspond to the minimum LCOE found for each heat exchanger and working fluid. As shown, regardless of the heat exchanger or working fluid, single-lateral designs with up to 20 km of horizontal drilling length at 5-km depth remain above $83/MWh$_e$ for a drilling cost of $1000/m.

Table 3
Minimum LCOE values for the considered parameter space over a 40-year operating period using a discount rate of 7 % and drilling cost of $1000/m. Corresponding maximum parameters include the rock thermal conductivity of 4.5 W/m K, vertical drilling depth of 5000 m, geothermal gradient of 0.07 °C/m, and borehole diameter of 0.4445 m (17.5 in.). For the sCO$_2$ results, the direct turbine expansion cycle required tuning the degree of pre-cooling and turbine outlet pressure (not listed).

System configuration	U-shaped		Coaxial	
Working fluid	Water	sCO$_2$	Water	sCO$_2$
Mass flow rate, kg/s	43	100	39.2	69.6
Horizontal extent, m	20,000	20,000	20,000	13,000
Injection temperature, °C	60	60	60	60
Average heat production, MW$_{th}$	26.0	22.2	23.8	14.1
Average electricity generation, MW$_e$	3.9	5.0	3.5	2.8
Conversion efficiency	0.15	0.23	0.15	0.2
Average production temperature, °C	205	190	203	174
Average production pressure, MPa	25.7	33.5	24.7	30.2
LCOE, $/MWh$_e$	96.6	83.0	93.5	86.9

Circulating sCO$_2$ through a u-shaped heat exchanger and then through a hypothetical direct turbine expansion cycle is the optimal CLGS design with respect to minimizing LCOE, as evidenced in Table 3. Here, a pre-cooling of 32 °C and a fixed turbine outlet pressure of 8.1 MPa (81 bar) have been used. This design results in a strong thermosiphon and converts 23 % of the thermal heat (22.2 MW$_{th}$) to electricity at an average production pressure and temperature of 33.5 MPa (335 bar) and 190 °C, respectively. We note this 23 % thermal efficiency is higher than what is typically found in existing ORC plants. LCOEs for this hypothetical system at drilling costs of $0/m, $500/m, and $1000/m are shown in Table 4. Evidently, to meet the 2035 DOE LCOE target of $45/MWh$_e$, the drilling cost associated with this 30-km, 0.4445-m (17.5-in.) borehole would need to be significantly reduced.

As an aside, we note that the highest mass flow rate considered in the HDF5 database is 100 kg/s. As such, the mass flow rate for this hypothetical sCO$_2$ example is not a true optimal flow rate. We expect higher flow rates could be used for circulating sCO$_2$ through a 0.4445-m (17.5-in.) borehole over a 20-km lateral length with a highly conductive formation and with bottom borehole temperatures of 375 °C. However, as explained earlier, this scenario is for illustration only and is far from physically reasonable. For more reasonable parameters, the 100 kg/s imposed upper limit does not prevent finding a true optimum flow rate for minimum LCOEs, as is shown subsequently.

We consider four examples to better understand what impact more conventional rock thermal conductivities and thermal gradients might have on the LCOE and to what extent lower drilling costs make these designs economically practical. For the following examples, we encourage the reader to use the *GeoCLUSTER* web app to follow along and vary the input parameters in real time to see the direct impact on

Table 4

Levelized cost of electricity (LCOE) for single-lateral designs at three drilling costs for the extremes of the database (first two rows) and corresponding LCOEs for the same designs with a reduced rock thermal conductivity and geothermal gradient (Examples 1–3). Here, the mass flow rate has been adjusted on a case-by-case basis to minimize LCOE.

	System configuration	Working fluid	Rock thermal conductivity, W/m K	Geothermal gradient, °C/m	LCOE $/MWh$_e$ $0/m drilling cost	$500/m drilling cost	$1000/m drilling cost
Table 3	u-shaped	sCO_2	4.5	0.07	36.9	60.0	83.0
Table 3	coaxial	water	4.5	0.07	38.8	66.1	94.0
Example 1	u-shaped	sCO_2	3.0	0.07	41.0	72.3	104.0
Example 2	u-shaped	sCO_2	3.0	0.045	42.0	120.4	199.0
Example 3	coaxial	water	3.0	0.045	45.0	145.0	246.0

various quantities of interest.

Example 1: In this example, we consider the same sCO_2 u-shaped design but reduce the rock thermal conductivity to 3 W/m K. With this reduction, the resulting value of $\frac{k}{\sqrt{\alpha}} = 2552$ J/m^2 s$^{1/2}$ K is representative of geothermal reservoirs in the western continental United States. Correspondingly, the average heat, power, production temperature, and outlet pressure drop to 17.7 MW$_{th}$, 3.6 MW$_e$, 160 °C, and 31.4 MPa (314 bar), respectively. As shown in Table 4, the LCOE at the $1000/m drilling cost is well above the DOE target. Indeed, even the free-drilling LCOE barely meets the 2035 DOE LCOE target for EGS. We note that this case required tuning the pre-cooling to 17.5 °C and turbine outlet pressure to 8.2 MPa (82 bar).

Example 2: In this example, we additionally lower the thermal gradient to a more reasonable value of 0.045 °C/m (45 °C/km), yielding a 250 °C bottom borehole temperature and markedly worse LCOEs. For context, a 0.045 °C/m (45.0 °C/km) geothermal gradient corresponds to 0.02 °C/m (20.0 °C/km) above the reported worldwide average (DiPietro, 2013). Using *GeoCLUSTER,* we adjust the mass flow rate, pre-cooling, and turbine outlet pressure to near optimal values of 86.6 kg/s, 5.5 °C, and 8.3 Mpa (83 bar), respectively, yielding average heat, power, production temperature, and pressure of 9 MW$_{th}$, 1.4 MW$_e$, 115 °C, and 27.5 MPa (275 bar), respectively.

As shown in Table 3, this trend of high LCOEs is not unique to the u-shaped heat exchanger or the sCO_2 circulating fluid. The physical limitations of HDR continue to result in prohibitive LCOEs when switching heat exchanger designs to a 0.4445-m (17.5-in.) coaxial heat exchanger circulating water at the same max depth (5 km) and lateral length (20 km), where now the heat is converted to electrical power using a generalized binary ORC. Revisiting Table 3, at these extremes we observe for an optimal mass flow rate of 39.2 kg/s average heat, power, production temperature, and production pressure of 23.8 MW$_{th}$, 3.5 MW$_e$, 203 °C, and 24.7 MPa (247 bar), respectively. In Table 4, we see once again that drilling costs would need to be significantly reduced to meet the 2035 DOE target of $45/MWh$_e$, despite using a hypothetical scenario that is not reflective of the geothermal resource base.

Example 3: In this example, we re-evaluate the same coaxial-heat exchanger design, but using a more reasonable rock thermal conductivity of 3 W/m K and thermal gradient of 0.045 °C/m (45.0 °C/km). With a near optimal mass flow rate of 37 kg/s, the average heat, power, production temperature, and production pressure are 10.8 MW$_{th}$, 922 kW$_e$, 130 °C, and 21.5 MPa (215 bar), respectively. Besides losing most of the thermosiphon due to the low average production temperature, the heat to power conversion efficiency also suffers and has dropped to 8.5 %.

Example 4: As a final example, we consider both heat exchangers emplaced in a geothermal reservoir that is representative of the geothermal resource base in the western continental United States. In addition to the fixed parameters of Table 1, this example uses a 0.07 °C/m (70 °C/km) geothermal gradient, rock thermal conductivity of 3.0 W/m K, vertical depth of 3.5 km (i.e., bottom borehole temperature of 270 °C), and a borehole diameter of 0.35 m. Both working fluids (water and sCO_2) are considered and are injected at 50 °C and 20 MPa (200 bar).

Fig. 7 plots the LCOE for this example from the western continental U.S. as a function of the horizontal lateral length and mass flow rate at a drilling cost of $1500/m. Here, the clipping shown in the left column is due to the minimum 100 °C production temperature requirement imposed by the ORC correlations used in *GeoCLUSTER*. Similarly, for the sCO_2 results, low production temperatures result in clipping (bottom right) due to low turbine outlet temperatures near the critical temperature. While this can be mitigated by increasing the turbine outlet pressure, this would severely reduce performance as optimal turbine outlet pressures are slightly above the critical pressure (Wang et al., 2021).

Fig. 7 indicates that different minimum LCOE values (and locations) are achieved due to differences in the heat exchangers, working fluids, and thermal heat to electrical power conversions (i.e., ORC for water vs. direct turbine expansion cycle for sCO_2); however, we again reach the similar conclusion that single-lateral heat exchangers with total drilling lengths under 30 km result in prohibitive LCOEs. Irrespective of the circulating fluid, LCOEs are 4.9 to 6.9 times the 2035 DOE target of $45/MWh$_e$. In fact, as shown in the LCOE contours in Fig. 8, even if the drilling cost was reduced to $100/m, neither heat exchanger circulating either fluid could meet the 2035 DOE target for EGSs with LCOEs between $3/MWh$_e$ and $15/MWh$_e$ above the target.

On a final note, both Figs. 7 and 8 show that for three of the four cases, the minimum LCOE falls on the max lateral length boundary with what appears to be a non-zero gradient, indicating that this 20-km max lateral length is not a true optimal design. On the other hand, the optimal mass flow rates (i.e., residency time) shown for these cases are below 100 kg/s and are indeed optimal for these heat exchangers. The former suggests that it is economic to consider systems with more than 30 km of total drilling length.

3.3.2. *LCOH for single-lateral designs*

The current U.S. average for energy content of natural gas, as reported by the U.S. Energy Information Administration (EIA), is around 1030 MBtu/MCF (302 kWh/MCF), and the current industrial price for natural gas, as reported by the EIA, varies but $8/MCF is representative, yielding an industrial heating cost of $0.0265/kWh$_{th}$ ($26.5/MWh$_{th}$). When accounting for the CAPEX and maintenance cost of the gas furnace, thermal inefficiencies, and cost of CO_2 emissions to be $185 per ton of CO_2 (Rennert et al., 2022), LCOHs closer to $40/MWh$_{th}$ may be considered economic. Using our database, we can assess whether direct use of the thermal heat from the considered CLGS designs will reach these target LCOHs. Instead of repeating the preceding examples, where we started with a hypothetical system that minimizes levelized costs and then transitioned to more physically reasonable reservoirs conditions, here we directly highlight the results for CLGSs emplaced in an HDR reservoir representative of the western continental U.S.

Fig. 9 plots the LCOH contours as a function of the mass flow rate and

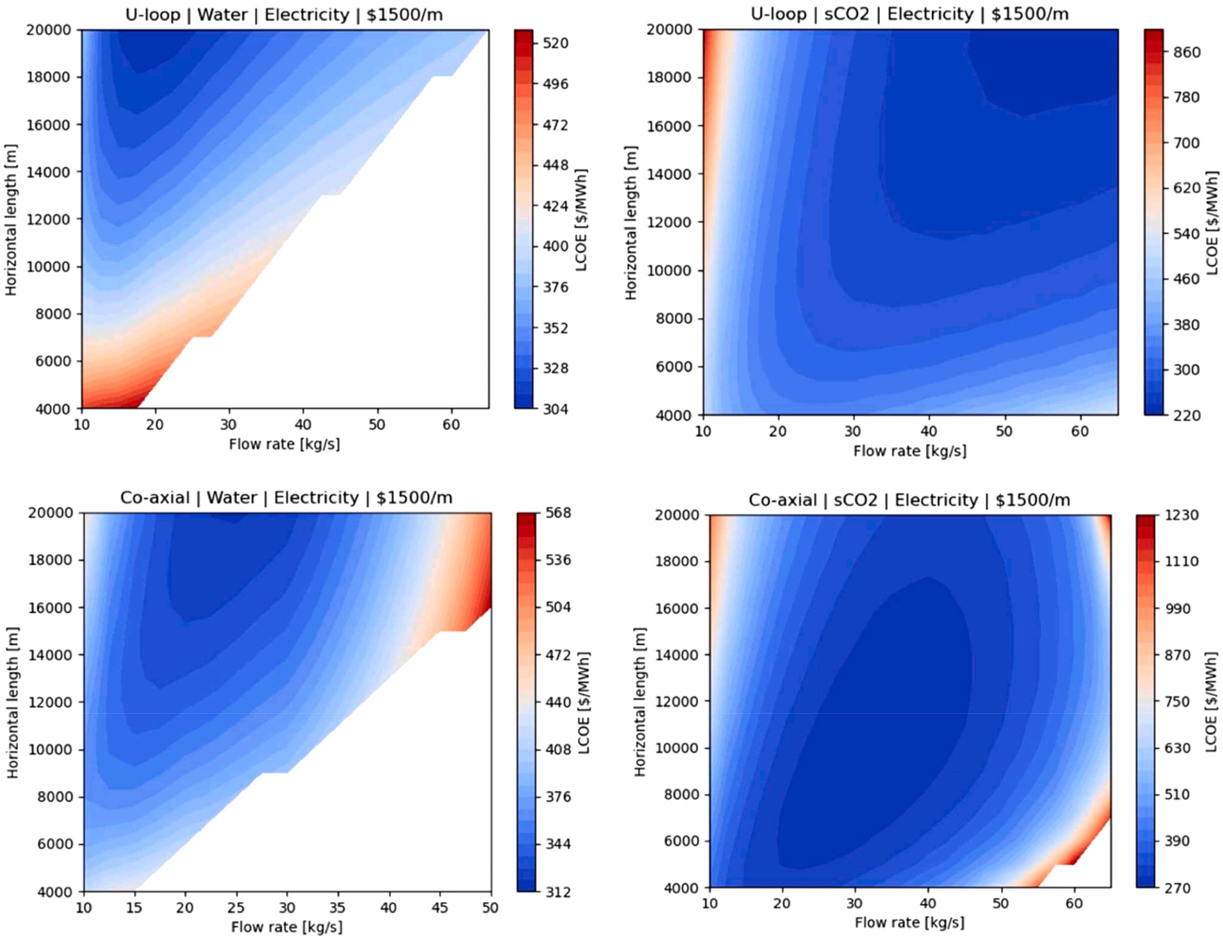

Fig. 7. Levelized cost of electricity (LCOE) at $1500/m drilling cost for u-shaped heat exchanger (top row) and coaxial heat exchanger (bottom row) emplaced in a representative geothermal reservoir of the western continental U.S. Each heat exchanger circulates either water (left column) or sCO_2 (right column). Water power output is computed using ORC correlations, whereas sCO_2 power output corresponds to a steady state direct turbine expansion cycle with the degree of pre-cooling and turbine outlet pressure tuned to maximize power output.

lateral length for the western continental U.S. example at a drilling cost of $1500/m for both heat exchangers and both working fluids. Compared to Fig. 7, the mass flow rate range here has been extended to the maximum database limit of 100 kg/s to highlight minimum LCOH locations. Immediately we see that an LCOH of less than $40/MW$_{th}$ can be reached for all combinations. Comparing heat exchangers, different design points are preferred. For the coaxial heat exchanger, excessive pressure drops (denoted by white regions) occur at high mass flow rates and long lateral lengths due to the smaller hydraulic diameters of the pipe-in-pipe system as compared to u-shaped design. Consequently, at this borehole diameter, the coaxial optimum strikes a balance between increased pumping costs and increased thermal output and favors intermediate lateral lengths and mass flow rates for both working fluids.

For the u-shaped configuration, the larger hydraulic diameter permits increased mass flow rates and longer lateral lengths, which, when increased in unison, tend to further decrease the LCOH (e.g., the gradient of the LCOH for water points toward the upper right corner). Evidently, for this example, the LCOH for the u-shaped configuration can be decreased by considering lateral lengths longer than the 20-km limit of our database and mass flow rates greater than the 100-kg/s limit of our database; however, the increased spacing between LCOH contours indicates that at these lengths and mass flow rates we are entering a zone of diminishing returns. On a final note, when comparing circulating fluids, water outperforms sCO_2 for both heat exchangers; however, the difference in minimum LCOHs is only $3–4/MWh$_{th}$ across the two considered heat exchanger designs and so is not substantial.

3.3.4. Comparing single- and multi-lateral U-shaped configurations

Using the SBT model, Beckers et al. (2022) evaluated the thermal and economic performance of u-shaped multi-lateral configurations by comparing 2-, 5-, and 13-lateral designs with water as the working fluid in addition to sCO_2 for the 2-lateral design. As the number of variable parameters considered for the suite of simulations was limited and our HDF5 CLGS HDR database does not specifically address multiple laterals, there is a current gap in available performance data for u-shaped multi-laterals. One might ask whether the single-lateral u-shaped configuration results could be applied to model a closed-loop multi-lateral configuration. To answer this, simulations were executed using the SBT model, comparing single- and three-lateral u-shaped configurations, where the overall borehole length was conserved, for both water and sCO_2 as the working fluid.

As an illustrative example, we consider a single-lateral system with a horizontal extent of 20 km (“U1”) and an equivalent three-lateral configuration of 6.66 km horizontal extent (“U3”) with 100-m spacing in between laterals. Fixed parameters include a mass flow rate of 40 kg/s, inlet temperature of 50 °C, inlet pressure of 20 MPa (200 bar), surface temperature of 20 °C, geothermal gradient of 0.07 °C/m (70 °C/km), rock thermal conductivity of 2.83 W/m K, rock specific heat of 825 J/kg K, rock density of 2875 kg/m^3, borehole diameter of 0.1524 m, pipe roughness of 10^{-6} m, and depth of 5 km.

Fig. 10 indicates that the outlet temperatures for both water and sCO_2 are nearly identical for the two configurations. However, as anticipated, the pressure drop across the three-lateral system is notably

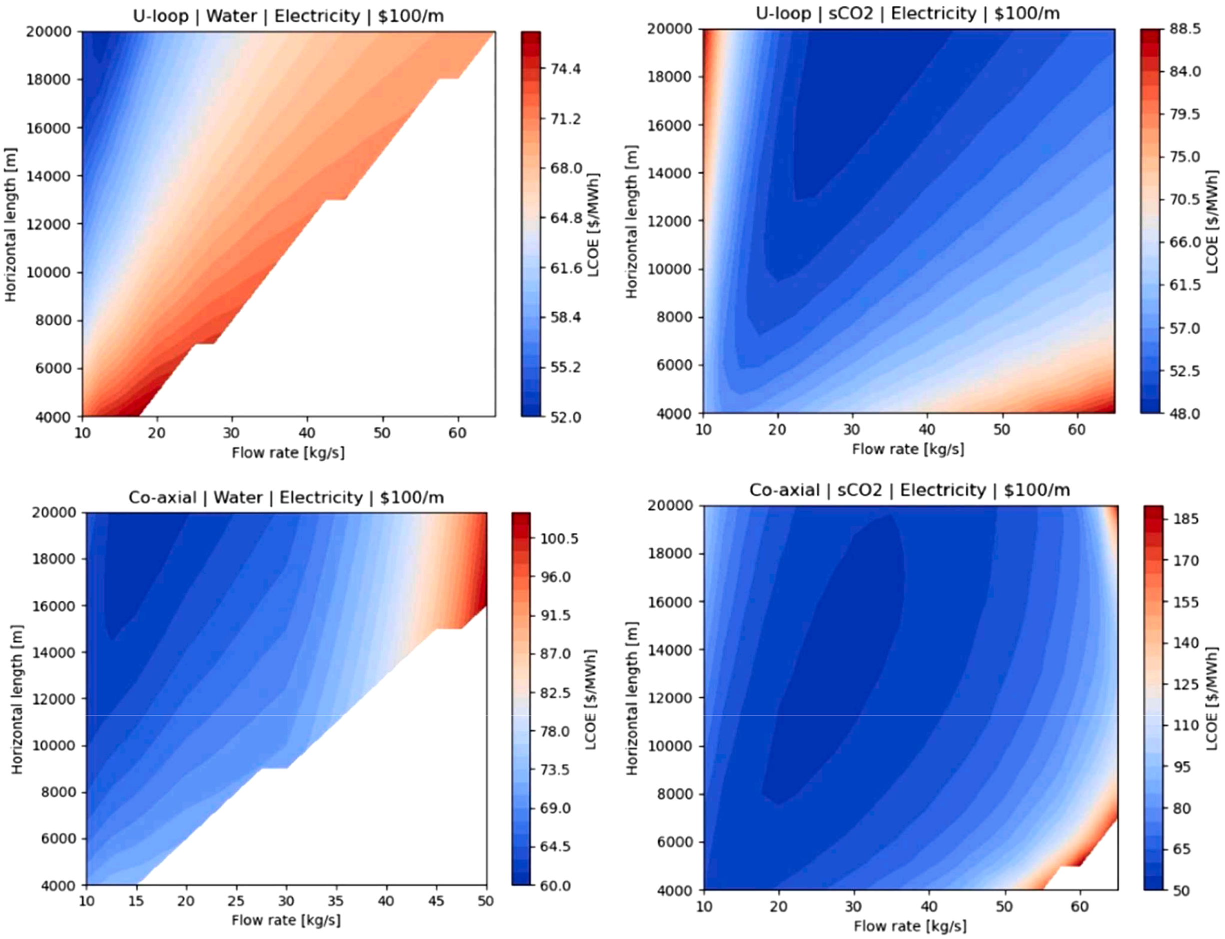

Fig. 8. Levelized cost of electricity (LCOE) at a reduced drilling cost of $100/m for u-shaped heat exchanger (top row) and coaxial heat exchanger (bottom row) emplaced in a representative geothermal reservoir of the western continental U.S. Each heat exchanger circulates either water (left column) or sCO_2 (right column). Water power output is computed using ORC correlations, whereas sCO_2 power output corresponds to a steady state direct turbine expansion cycle with the degree of pre-cooling and turbine outlet pressure tuned to maximize power output.

less. The corresponding produced enthalpy and exergy (available power) are plotted Fig. 11. These results suggest that the results found in *GeoCLUSTER* for produced heat for single laterals can be transferred to multi-lateral configurations for the same total borehole length, assuming sufficient spacing between laterals to avoid thermal interference. However, the results for electricity generation in *GeoCLUSTER* for single-lateral systems may be an underprediction when considering multi-laterals with the same total borehole length.

3.3.5. *Case study of multi-lateral coaxial configurations*

Using the INL model, a single long vertical coaxial section split into several lateral horizontal legs (Wang et al., 2022) emplaced in HDR and circulating water was modeled. Although this concept has not been demonstrated as technically achievable, advances in the oil and gas industry over the last decade hold promise that this configuration is possible (Husain et al., 2011; Ghadami et al., 2022; Almedallah et al., 2021). Compared to a u-shaped configuration, this multi-leg system has the advantage of minimizing the number of drilling locations and containing the external infrastructure costs. On the other hand, it is more complex to realize because of the installation of the internal casings that keep hot/cold water flows separated.

Configurations with 1, 2, 4, 8, and 16 laterals were modeled using the computational domains shown in Fig. 12. Considering the limited radial dimensions of the borehole (<1 m) compared to the radial extent of the domain (200 m), the rock domain has been modeled as continuous (i.e., no hole). This approximation has proved to save computational time (i.e., mesh simplification) without compromising accuracy. The wetted perimeter of the borehole is used to define the zone of heat transfer between the rock domain and the borehole/water.

We consider the INEL-1 site with a vertical borehole depth of 4728 m. The INEL-1 site is located on the INL complex, a 980-mi^2 area very close to the Yellowstone caldera and part of the Snake River Plain. Geologic data for the INEL-1 site was based on the geothermal characteristics of the INEL-1 well (Doherty et al., 1979; Mann, 1986; Blackwell et al., 2011). Information on the geological characteristics has been obtained by drilling the INEL-1 well, which is 3159 m (10,365 ft) deep and is characterized by a gradient of 0.044 °C/m (44 °C/km). The INEL-1 well geological stratigraphy is composed of layers of volcanic rock, with basaltic lava flow and interbedded sediments down to a depth of 762 m. Rhyolitic welded ash-flow of tuffs/air-fall ash deposits and non-welded ash-flow tuffs are instead composing the geological layers below 762 m. The low hydraulic conductivity found at the bottom of the well (2 x 10^{-6} cm/s) suggests that the HDR is a good approximation. A rock thermal conductivity of 3.05 W/m K, inlet temperature of 50 °C, lateral extent of 2511 m, and outer diameter of the vertical borehole of 0.254 m were used.

Using water as the working fluid, simulations were executed with the five configurations of laterals (i.e., 1 to 16) for four mass flow rates (i.e., 5, 10, 20, 40 kg/s). Total flow area was held constant across the lateral configurations to assure constant flow velocity with the inner tubing and annular space (i.e., mass flow was equally divided between laterals). As shown in Fig. 13 (upper plots), outlet temperatures and pressures for

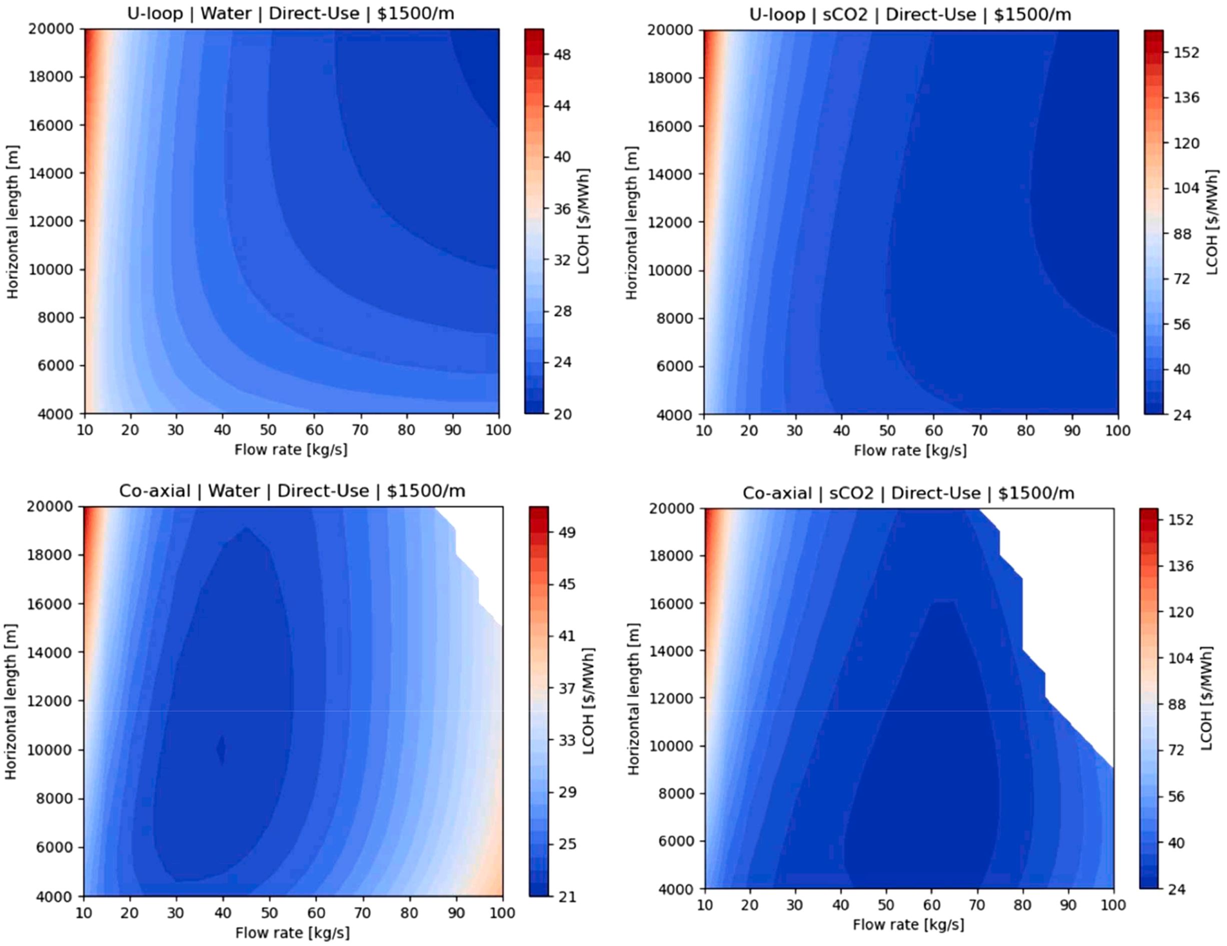

Fig. 9. Levelized cost of heat (LCOH) at a drilling cost of $1500/m for the u-shaped heat exchanger (top row) and coaxial heat exchanger (bottom row) emplaced in a representative geothermal reservoir of the western continental U.S. Each CLGS design circulates either water (left column) or sCO_2 (right column). Here, the clipping in the coaxial LCOH contours is due to excessive pressure drops caused by the small hydraulic diameters.

mass flow rates of 20 and 40 kg/s display the classical forms (i.e., a transient period, early in time, with a sharp decline in temperature, followed by a slower decline in temperature) with respect to outlet conditions versus time, surface area, and mass flow rate. Increasing lateral count yields decreasing mass flow rates in the individual laterals while simultaneously increasing lateral surface area (i.e., lateral surface area increases by the square root of the number of laterals). Due to increased residence time, the outlet temperatures increase with lateral count. At 20 kg/s, the system transitions from thermo-siphoning to requiring pumping with decreasing lateral count, with the transition occurring between four and two laterals (Fig. 13, middle left plot). At 40 kg/s, the increased flow rates and lower outlet temperature yield conditions that require active pumping (Fig. 13, middle right plot). Simulation results for 16 laterals at 40 kg/s yielded unstable boiling conditions and were not reported. With water as the working fluid, produced thermal power (i.e., $m\ \Delta h$) reflects the outlet temperature versus time (Fig. 13, lower plots).

Table 5 tabulates the LCOH and LCOE for the INEL-1 site while varying the number of laterals and the mass flow rate. Here, a drilling cost of $1000/m is assumed with an operational period of 20 years. Additional economic parameters are set to the *GeoCLUSTER* default values. Table 5 indicates that the preferred system design for direct use has eight laterals with a mass flow rate of 40 kg/s. This option offers the lowest LCOH with average production temperatures of 151.4 °C, owing to the lower mass flow rates per lateral. Similarly, the preferred system design for electricity generation has eight laterals; however, since the thermal heat is converted to power using an ORC, the preferred mass flow rate is now 20 kg/s such that higher production temperatures are achieved (see Fig. 13). Table 5 indicates that this design and other considered designs do not meet the 2035 DOE LCOE target of $45/MWh$_e$. Lastly, although not shown here, we found similar results when considering a reservoir with higher gradients [i.e., 0.0788 °C/m (78.8 °C/km)] modeled after the Utah FORGE site. Whereas both the INEL-1 and FORGE sites had economic potential for direct use, neither site had economic potential for generating electricity.

3.3.5. Alternative designs and settings

A fundamental challenge to deep CLGS is that heat transport from the hot reservoir to the circulating working fluid relies on conduction through rock, which is a relatively poor conductor. One concept to overcome this limitation would be to create hydraulic fractures along the length of the borehole, and then fill those fractures with conductive material, conceptually similar to the fins on radiators of hydronic heating systems. This system was proposed by (Ahmadi and Dahi-Taleghani, 2017) and then analyzed by Fowler and McClure (2021). The geomechanics of creating hydraulic fractures along the length of the borehole, places an upper limit on the total thickness of fractures along the borehole, which in turn limits the heat conduction along the fractures into the circulating working fluid. Another concept would be to drill a larger diameter borehole and then fill the void between the circulating fluid pipe wall and borehole with conductive material. This approach was considered using axisymmetric modeling system shown in Fig. 2 and reported in Appendix B: Conductive Material Enhancement. The results from this study indicate a 1 m thick zone around the borehole

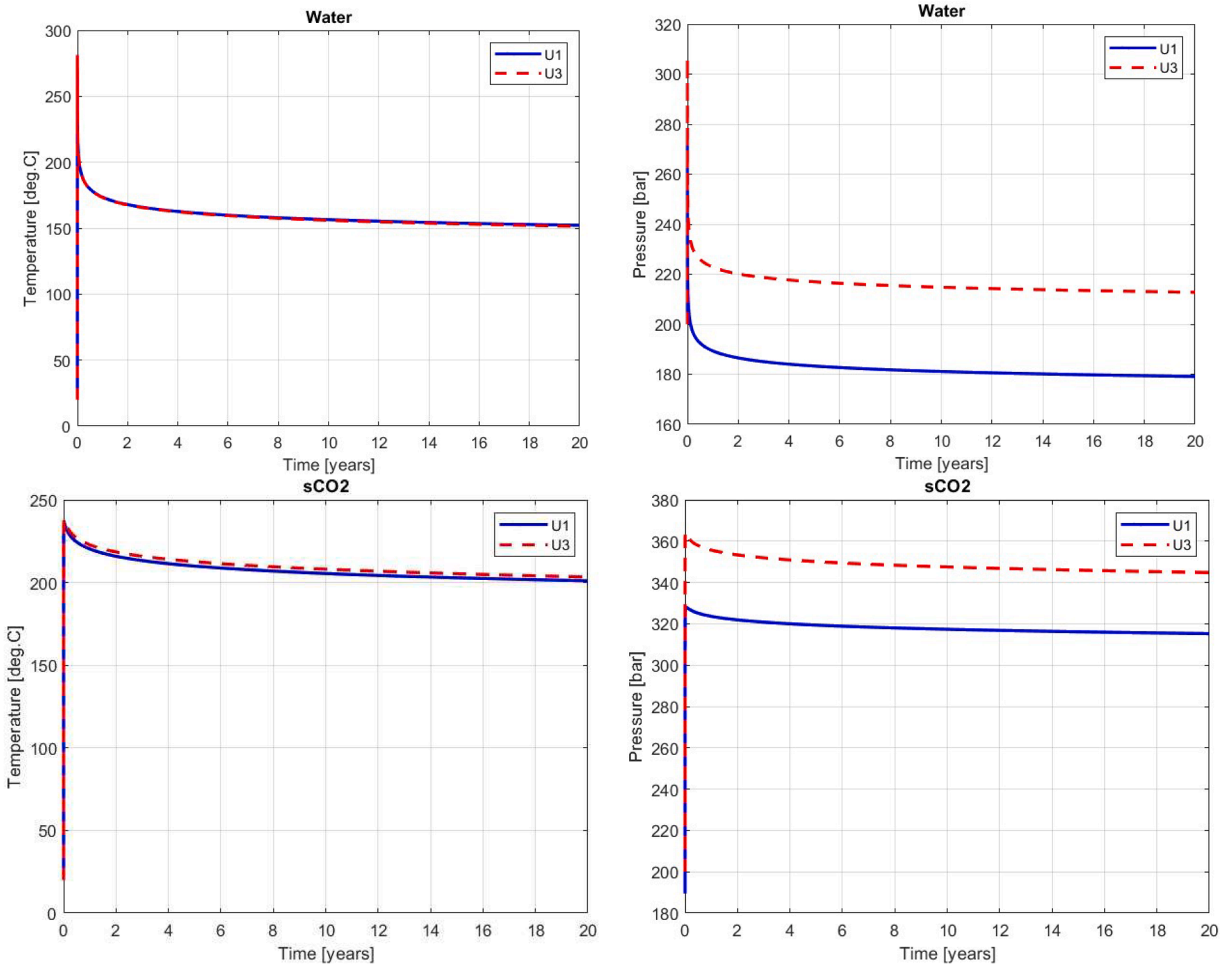

Fig. 10. Outlet temperature (left) and pressure (right) for single- and three-lateral u-shaped configurations with water (top) and sCO_2 (bottom) as the working fluid.

could at most increase the average available power and average thermal power by a factor of 1.6 and 1.5, respectively.

Other concepts involve incorporating natural convection along or across the closed-loop heat exchanger pipe. Two designs that involve flow along the pipe, start with vertical well with an open annulus outside the closed-loop heat exchanger pipe. In one design, a natural convection cell is generated by creating a water-filled vertical fracture along the length of the borehole, creating a circulation path down the annulus, returning upward via heating in the fracture. Technical barriers to this design its use of a single fracture and the low driving forces for free convection (McClure, 2023). In the second design the annulus is open to a steam-filled reservoir (Higgins et al., 2021), and steam condensation on the heat-exchanger wall creates the natural convection driving force. Whereas condensing steam yields high heat transfer rates, this technology is limited to very specific geologic settings, which are not prevalent across the continental United States. An alternative natural convection system would be that of a horizontal closed-loop heat exchanger pipe emplaced in a permeable formation (i.e., hot-wet-rock). This system was modeled numerically and reported in Appendix C: U-Shaped Configurations in Permeable Wet Rock, considering the impact of rock permeability, borehole diameter, and depth.

4. Conclusions

Comparisons of simulation results from four independent computer codes of two common CLGS heat exchanger designs (coaxial and u-shaped) emplaced in HDR confirmed results of previous work showing that computationally inexpensive 2D axisymmetric models can accurately simulate these closed-loop systems. Using these 2D axisymmetric models, 2.5 million HDR system configurations were simulated across these two heat exchangers, two working fluids (sCO_2 and water), and seven independent parameters chosen to cover a wide range of both conventional and hypothetical systems. The resulting below-ground HDF5 database was combined with an above-ground plant and economic model and wrapped into a single techno-economic web application. The web app is tailored to a general audience and is publicly accessible at https://gdr.openei.org/submissions/1473.

Using the developed database, we assessed the LCOE and LCOH across simulations in the database. When compared to the current cost of heat, estimated to be between $26.5/$MW_{th}$ and $40/$MW_{th}$ for natural gas, we found that both heat exchangers with either water or sCO_2 as the working fluid could meet these current targets with minimal LCOHs found between $20/$MW_{th}$ to $24/$MW_{th}$ across different designs at a drilling cost of $1500/m.

At a $1000/m drilling cost, the lowest LCOE we found was $83/$MWh_e$, corresponding to a hypothetical system circulating sCO_2 through a 17.5-in. u-shaped configuration drilled to a maximum depth of 5 km with a maximum lateral length of 20 km. This 30-km CLGS uses a direct turbine expansion cycle to generate power and is exposed to a thermal gradient of 0.07 °C/m (70 °C/km) and a rock thermal conductivity of 4.5 W/m K such that $\frac{k}{\sqrt{\alpha}} = 3127$ J/m^2 s$^{1/2}$ K. With these extreme parameters, this "what if" scenario converts nearly 23 % of the thermal heat (22.2 MW_{th}) to power (5 MW_e) at an average production pressure and temperature of 33.5 MPa (335 bar) and 190 °C, respectively. However, despite the extreme parameters, this system still fails to meet the 2035 DOE LCOE target of $45/$MWh_e$ unless drilling costs are

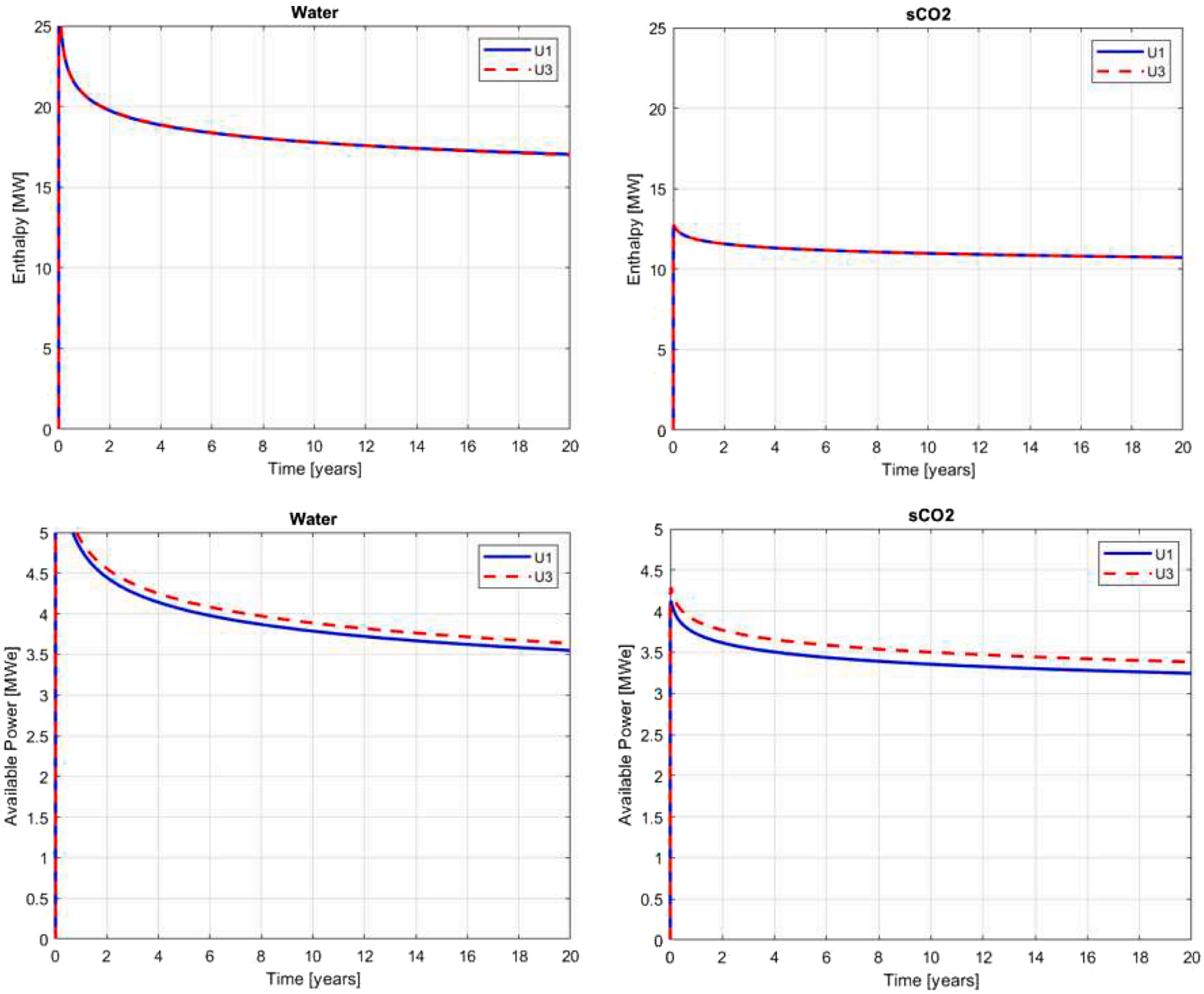

Fig. 11. Produced enthalpy and maximum available power (exergy) for U1 and U3 scenarios for both water and sCO_2. For the same total borehole length, no difference is observed in enthalpy produced. However, a small increase is observed in available power due to higher production pressures in the U3 scenario vs. the U1 scenario.

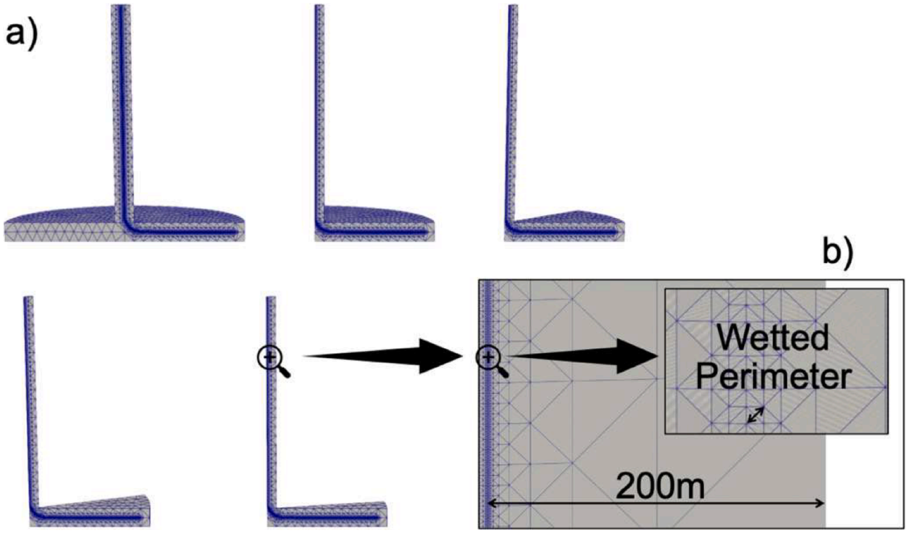

Fig. 12. (a) Computational domain for a coaxial configuration with multiple laterals from 1 to 16, (b) detail of the mesh refinement. As shown, the rock domain has a radial dimension of ~200 m. Previous analyses (Parisi et al., 2021) demonstrated that this length is sufficient to enclose the thermal drawdown. Here, the lateral extent is 2511 m. Considering the limited radial dimensions of the borehole (<1 m) compared to the lateral dimensions of the system (200 m), the rock domain has been modeled as a continuous domain (no hole). This approximation has proved to be efficient in saving computational time (mesh simplification) without compromising the results accuracy. The wetted perimeter of the borehole is used to define the zone of heat transfer between the rock domain and the borehole/water.

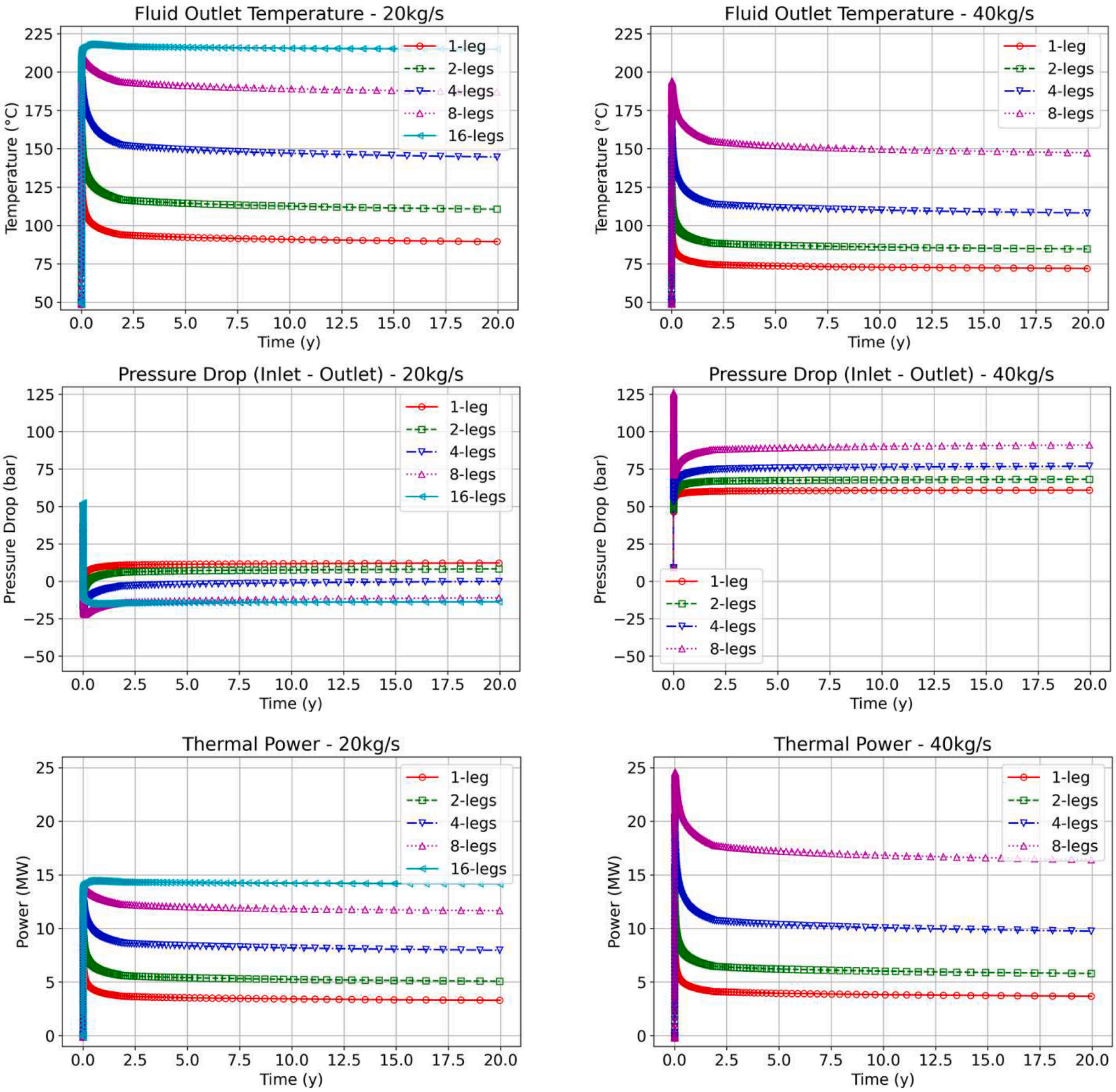

Fig. 13. Water outlet temperature (upper plots), pressure (middle plots), and thermal power (lower plots) at various lateral counts for 20 (left plots) and 40 (right plots) kg/s for the INEL-1 site.

significantly reduced.

When emplacing the CLGS in HDR that is more representative of the geothermal resource base in the western continental U.S., we find that across heat exchangers and working fluids, LCOEs are between 4.9 to 6.9 times the 2035 DOE LCOE target, assuming a drilling cost of $1500/m. Indeed, even when drilling costs are reduced to $100/m, irrespective of the working fluid or heat exchanger, all single-lateral designs have LCOEs between $3/MWh$_e$ to $15/MWh$_e$ above the $45/MWh$_e$ target LCOE.

Our HDR results should come as no surprise, as much earlier studies by Ramey (1962) for u-shaped configurations and Horne (1980) for coaxial configurations, as well as later studies by Nalla et al. (2005) and others, demonstrated that production temperatures in HDR decay over time and become much lower than the neighboring rock temperature imposed by the thermal gradient. Production temperatures of CLGSs in HDR reservoirs follow a specific temporal behavior—a transient period, early in time, with a sharp decline in temperature, followed by a slower decline in temperature. These characteristics stem from conduction through reservoir rock being the dominant heat transfer mechanism in CLGS. The physical behavior of CLGS is well understood and there are limited steps that can be taken to increase thermal and useful energy output, the primary one being to increase the surface of the CLGS in contact with the rock reservoir. This is usually achieved by making the borehole longer and/or increasing its diameter. Both normally come at an increased capital cost. Even under the most favorable conditions, the energy output of CLGS wells is usually less than that of a typical conventional hydrothermal well. The main factor in CLGS project economics is the cost of drilling and completing the CLGS, and whether the energy production justifies the drilling expense.

With respect to longer boreholes, multi-lateral designs are promising as the respective pressure drops are lower than the equivalent single-lateral systems. However, our multi-lateral coaxial case study for the INEL-1 site indicated that at a target depth of 5 km with a 0.044 °C/m (44 °C/km) gradient, and thermal conductivity of 3.05 W/m K, the 2035 DOE target LCOE could not be met despite totaling to almost 30 km of drilling. A similar conclusion was found for multi-laterals emplaced at the more favorable FORGE site, but these results are not provided here. For more general multi-lateral cases, we showed that our single-lateral

Table 5
Economic analyses for the multi-lateral coaxial configuration circulating water at the INEL-1 site.

Number of laterals	Drilling length (m)	Flow rate (kg/s)	CAPEX for LCOH (M$)	CAPEX for LCOE (M$)	LCOH ($/MWh$_{th}$)	LCOE ($/MWh$_e$)
1	11,270	5	11.6	12.2	48.2	577
2	13,780	5	14.1	15	46.5	433
1	11,270	10	11.7	12.1	37.9	696
2	13,780	10	14.3	15.4	32.8	444
4	18,801	10	19.5	21.3	32.9	324
8	28,844	10	29.6	31.6	42	357
16	48,929	10	49.7	51.8	68.1	554
1	11,270	20	11.7	11.3	34.3	–
2	13,780	20	14.5	15.1	27.4	593
4	18,801	20	19.8	21.8	23.9	345
8	28,844	20	30.2	33.9	25.4	254
16	48,929	20	50.4	54.5	35.7	305
1	11,270	40	11.8	11.3	39.8	–
2	13,780	40	14.6	13.8	30.3	–
4	18,801	40	20.1	21.4	23.9	1693
8	28,844	40	30.9	35.2	21.2	399

CLGS HDR database can be used to estimate performance of equivalent u-shaped multi-lateral systems up to a total drilling length of 30 km for either water or sCO_2, where for the latter it will underpredict performance.

Excluding substantial drilling cost reductions, we suspect economic HDR designs for electricity production are CLGS multi-lateral designs at depths greater than the 5 km considered here while simultaneously exposed to favorable gradients near 0.07 °C/m (70 °C/km). The working fluid is not a limiting factor and either water or sCO_2 could be used, though results indicate sCO_2 with a (hypothetical) direct turbine expansion cycle would result in a more efficient power cycle as compared to existing ORC binary plants. More importantly, we expect total drilling lengths of such a system to be closer to 100 km than the 30-km total length limit considered here, neither of which have been demonstrated in the field, irrespective of the drilling cost.

Lastly, the heat transfer limitations of conduction may be overcome in water/brine-saturated permeable geothermal reservoirs via natural convection, induced by the density differences in water/brine with temperature. For an example u-shaped configuration studied, we found the average available power production over 25 years improves from 723 kW$_e$ for a conduction-dominated reservoir to 2187 kW$_e$ and 3586 kW$_e$ for water/brine saturated reservoirs with intrinsic permeabilities of 500 and 2000 mD, respectively. It is noted that rather generous values were specified for permeability, geothermal gradient, and tubing diameter. Our results indicate that 500 mD or greater can substantially enhance power production as compared to HDR; however, natural permeabilities of 2000 mD are not common for sedimentary rock (e.g., Table 2 in Martinez and Hesse, 2016) and are even less likely at depths of 3 to 5 km. Hydraulic fracturing or use of existing, previously fractured idle or abandoned wells could be attractive for harnessing buoyant convection for enhanced harvesting of heat from the subsurface with CLGSs; however, in this case it may make more sense to use an open or EGS system.

CRediT authorship contribution statement

Mark White: Conceptualization, Software, Validation, Formal analysis, Writing – original draft. **Yaroslav Vasyliv:** Methodology, Software, Validation, Formal analysis, Data curation, Writing – original draft. **Koenraad Beckers:** Methodology, Software, Validation, Formal analysis, Data curation, Writing – original draft. **Mario Martinez:** Methodology, Software, Validation, Formal analysis, Data curation, Writing – original draft. **Paolo Balestra:** Methodology, Software, Validation, Formal analysis, Writing – original draft. **Carlo Parisi:** Methodology, Software, Validation, Formal analysis, Writing – original draft. **Chad Augustine:** Conceptualization, Formal analysis, Resources, Investigation, Writing – original draft, Supervision. **Gabriela Bran-Anleu:** Formal analysis, Writing – original draft. **Roland Horne:** Conceptualization, Formal analysis, Resources, Writing – review & editing, Supervision. **Laura Pauley:** Conceptualization, Writing – review & editing, Supervision. **Giorgia Bettin:** Writing – review & editing, Supervision, Project administration. **Theron Marshall:** Writing – review & editing, Supervision, Project administration. **Anastasia Bernat:** Software, Data curation, Writing – original draft.

Declaration of Competing Interest

The authors declare that they have no known competing financial interests or personal relationships that could have appeared to influence the work reported in this paper.

Data availability

Data from this research will be available on the Geothermal Data Repository.

Acknowledgments

This material was based on work supported by the U.S. Department of Energy, Office of Energy Efficiency and Renewable Energy, Geothermal Technologies Office, under contract numbers DE-AC05-76RL01830 with PNNL, DE-NA0003525 with Sandia National Laboratories, DE-AC07-05ID14517 with Idaho National Laboratory, and DE-AC36-08GO28308 with National Renewable Energy Laboratory. The United States Government retains, and the publisher, by accepting the article for publication, acknowledges that the United States Government retains a non-exclusive, paid-up, irrevocable, world-wide license to publish or reproduce the published form of this manuscript, or allow others to do so, for United States Government purposes. This work is guided by an expert panel comprising Roland Horne (Stanford University), Laura Pauley (Pennsylvania State University), and Chad Augustine (National Renewable Energy Laboratory), and Doug Hollett (Melroy-Hollett Technology Partners). We recognize and appreciate their dedication to the study and have greatly benefitted from their suggestions and reviews of the work.

Supplementary materials

Supplementary material associated with this article can be found, in the online version, at doi:10.1016/j.geothermics.2023.102852.

References

Adams, B.M., Bohnhoff, W.J., Dalbey, K.R., Ebeida, M.S., Eddy, J.P., Eldred, M.S., Hooper, R.W., Hough, P.D., Hu, K.T., Jakeman, J.D., Khalil, M., Maupin, K.A., Monschke, J.A., Ridgway, E.M., Rushdi, A.A., Seidl, D.T., Stephens, J.A., Swiler, L.P., and Winokur, J.G., 2021. *Dakota, A Multilevel Parallel Object-oriented Framework for Design Optimization, Parameter Estimation, Uncertainty Quantification, and Sensitivity Analysis: Version 6.15 User's Manual*, SAND2020-12495.

Ahmadi, M., Dahi-Taleghani, A., 2017. Thermoporoelastic analysis of a single-well closed-loop geothermal system. In: Proceedings, Poromechanics VI. Sixth Biot Conference on Poromechanics. Paris, France.

Almedallah, M., Altaheini, S.K., Clark, S., Walsh, S., 2021. Combined stochastic and discrete simulation to optimise the economics of mixed single-horizontal and multilateral well offshore oil developments. Pet. Explor. Dev. 48 (5), 1183–1197.

Augustine, C.R., 2009. *Hydrothermal Spallation Drilling and Advanced Energy Conversion Technologies For Engineered Geothermal systems*, Doctoral dissertation. Massachusetts Institute of Technology.

Barker, B.J., Gulati, M.S., Bryan, M.A., Riedel, K.L., 1991. Geysers Reservoir Performance. Monograph on the Geysers Geothermal Field. Geothermal Resources Council, pp. 167–177. Special Report No. 17.

Beckers, K.F., Rangel-Jurado, N., Chandrasekar, H., Hawkins, A.J., Fulton, P.M., Tester, J.W., 2022. Techno-economic performance of closed-loop geothermal systems for heat production and electricity generation. Geothermics 100. https://doi.org/10.1016/j.geothermics.2021.102318.

Beckers, K.F., Johnston, H.E., 2022. Techno-economic performance of Eavor-Loop 2.0. In: Proceedings, 47th Workshop on Geothermal Reservoir Engineering, Stanford, California, February 7–9, 2022. SGP-TR-223.

Beckers, K.F., McCabe, K., 2019. GEOPHIRES v2.0: updated geothermal techno-economic simulation tool. Geotherm. Energy 7 (1), 1–28.

Beckers, K.F., Koch, D.L., Tester, J.W., 2015. Slender-body theory for transient heat conduction: theoretical basis, numerical implementation and case studies. Proc. R. Soc. A 471, 20150494. https://doi.org/10.1098/rspa.2015.0494.

Beckers, K.J.H.F., 2016. Low-Temperature Geothermal Energy: Systems Modeling, Reservoir Simulation, and Economic Analysis. Cornell University.

Beckers, K., Vasyliv, Y., Bran-Anleu, G.A., Martinez, M., Augustine, C., White, M., Group, C.L.G.W., 2023. Tabulated database of closed-loop geothermal systems performance for cloud-based technical and economic modeling of heat production and electricity generation. In: Proceedings, 48th Workshop on Geothermal Reservoir Engineering, Stanford University, Stanford, California, February 6–8, 2023. SGP-TR-224.

Bell, I.H., Wronski, J., Quoilin, S., Lemort, V., 2014. Pure and pseudo-pure fluid thermophysical property evaluation and the open-source thermophysical property library CoolProp. Ind. Eng. Chem. Res. 53 (6), 2498–2508. https://doi.org/10.1021/ie4033999.

Blackwell, D., Richards, M., Frone, Z., Batir, J., Ruzo, A., Dingwall, R., Williams, M., 2011. Temperature at depth maps for the conterminous US and geothermal resource estimates. GRC Trans. 35, GRC1029452.

Brown, D.W., Duchane, D.V., Heiken, G., Hriscu, V.T., 2012. Mining the Earth's Heat: Hot Dry Rock Geothermal Energy. Springer. https://doi.org/10.1007/978-3-540-68910-2. ISBN 978-3-540-67316-3.

Budiono, A., Suyitno, S., Rosyadi, I., Faishal, A., Ilyas, A.X., 2022. A systematic review of the design and heat transfer performance of enhanced closed-loop geothermal systems. Energies 15, 742. https://doi.org/10.3390/en15030742.

DiPetro, J.A., 2013. Landscape Evolution in the United States. Elsevier. https://doi.org/10.1016/B978-0-12-397799-1. ISBN: 9780123977991.

DOE, 2022. "DOE launches new energy earthshot to slash the cost of geothermal power," Energy.gov, September 8, 2022, https://www.energy.gov/articles/doe-launches-new-energy-earthshot-slash-cost-geothermal-power, accessed 1 March 2023.

Doherty, D., McBroome, L., Kuntz, M., 1979. Preliminary Geological Interpretation and Lithologic Log of the Exploratory Geothermal Test Well (INEL-1). Idaho National Engineering Laboratory, Eastern Snake River Plain, Idaho. U.S. Geological Survey, Open-File Report, 79-1248.

Fowler, G., McClure, M., 2021. A feasibility study on three geothermal designs: deep closed-loop (with and without conductive fractures) and open-loop circulation between multifractured laterals. GRC Trans. 45, 635–653.

Gaston, D.R., Permann, C.J., Peterson, J.W., Slaughter, A.E., Andrš, D., Wang, Y., Short, M.P., Perez, D.M., Tonks, M.R., Ortensi, J., Zou, L., Martineau, R.C., 2015. Physics-based multiscale coupling for full core nuclear reactor simulation. Ann. Nucl. Energy 84, 45–54.

Ghadami, S., Biglarian, H., Beyrami, H., Salimi, M., 2022. Optimization of multilateral well trajectories using pattern search and genetic algorithms. Engineering 16, 100722.

Gnielinski, V., 1975. Neue gleichungen für den wärmeund den stoffübergang in turbulent durchströmten rohren und kanälen. Forsch. Ing. 41 (1), 8–16.

Hagoort, J., 2005. Prediction of wellbore temperatures in gas production wells. J. Pet. Sci. Eng. 49 (1–2), 22–36.

Higgins, B., Scherer, J., Amaya, A., Chandresekar, H., Van Horn, A., 2021. Closed-loop geothermal in steam dominated reservoirs. GRC Trans. 45, 14–24.

Hueze, F.E., 1983. High-temperature mechanical, physical and thermal properties of granitic rock—A review. Int. J. Rock Mech. Min. Sci. Geomech. Abstr. 20 (1), 3–10.

Horne, R.N., Shinohara, K., 1979. Wellbore heat loss in production and injection wells. J. Pet. Technol. 31 (1), 116–118.

Horne, R., 1980. Design considerations of a down-hole coaxial geothermal heat exchanger. Geotherm. Resour. Counc., Trans. 4.

Husain, T.M., Leong, L.C., Saxena, A., Cengiz, U., Ketineni, S., Khanzhode, A., and Muhamad, H., 2011. "Economic comparison of multi-lateral drilling over horizontal drilling for Marcellus shale field development," EME 580: Integrative Design of Energy & Mineral Engineering Systems, final project report, State College, PA.

Incropera, F.P., DeWitt, D.P., 2007. Fundamentals of Heat and Mass Transfer, sixth ed. Wiley, Hoboken.

Lowry, T., Finger, J., Carrigan, C., Foris, A., Kennedy, M., Corbet, T., Doughty, C., Pye, S., Sonnenthal, E., 2017. GeoVision Analysis Supporting Task Force Report: Reservoir Maintenance and Development. Sandia National Laboratories, Albuquerque, NM. SAND2017-9977.

Mann, L., "Hydraulic properties of rock units and chemical quality of water for INEL-1 a 10,354-foot-deep test hole drilled at the Idaho National Engineering Laboratory, Idaho", *U.S. Geological Survey, Water-Resources Investigations Report*, 86-4020, Idaho Falls, ID (1986).

McClure, M. "Technical barriers for deep closed-loop geothermal." *Available online:* https://www.resfrac.com/blog/technical-barriers-for-deep-closed-loop-geothermal (accessed on 5 September 2023).

Morita, K., Yamaguchi, T., Karasawa, H., Hayamizu, H., 1984. Development and evaluation of temperature simulation code for geothermal wells-prediction of temperature behavior in and around geothermal wells (1st report),. J. Min. Metall. Inst. Jpn. 100 (1161), 1045–1051.

Morita, K., Matsubayashi, O., 1986. The effect of major design parameters on the performance of a downhole coaxial heat exchanger - studies on the downhole coaxial heat exchanger (1st report). J. Geotherm. Res. Soc. Jpn. 8 (3), 301–322.

Martinez, M.J., Hesse, M.A., 2016. Two-phase convective CO2 dissolution in saline aquifers. Water Resour. Res. 52, 585–599. https://doi.org/10.1002/2015WR017085.

Morita, K., Bollmeier, W.S., Mizogami, H., 1992a. Analysis of the experimental results from the DCHE experiment was carried out to investigate the insulation performance of the inner pipe and the heat transfer characteristics in the formation. Geotherm. Resour.Counc., Trans. 16.

Morita, K., Bollmeier, W.S., Mizogami, H., 1992b. An experiment to prove the concept of the downhole coaxial heat exchanger (DCHE) in Hawaii. Geotherm. Resour.Counc., Trans. 16.

Munson, B.R., Rothmayer, A.P., Okiishi, T.H., Huebsch, W.W., 2013. Fundamentals of Fluid Mechanics, seventh ed. John Wiley & Sons, Inc., Hoboken, New Jersey.

Nalla, G., Shook, G.M., Mines, G.L., Bloomfield, K.K., 2005. Parametric sensitivity study of operating and design variables in wellbore heat exchangers. Geothermics 34, 330–346. https://doi.org/10.1016/j.geothermics.2005.02.001.

Oldenburg, C.M., Pan, L., Muir, M.P., Eastman, A.D., Higgins, B.S., 2016. Numerical simulation of critical factors controlling heat extraction from geothermal systems using a closed-loop heat exchange method. In: Proceedings, 41st Workshop on Geothermal Reservoir Engineering, Stanford University, Stanford, California, February 22–24, 2016. SGP-TR-209.

Pan, L., Oldenburg, C.M., Wu, Y., Pruess, K., 2011. T2Well/ECO2N Version 1.0: Multiphase and Non-Isothermal Model For Coupled Wellbore-Reservoir Flow of Carbon Dioxide and Variable Salinity Water. Lawrence Berkeley National Laboratory, Berkeley, California. LBNL- 4291E.

Pan, L., Spycher, N., Doughty, C., Pruess, K., 2014. ECO2N V. 2.0: A New TOUGH2 Fluid Property Module for Mixtures of Water, NaCl, and CO_2. Lawrence Berkeley National Laboratory, Berkeley, California. LBNL-6930E.

Parisi, C., Balestra, P., Marshall, T.D., 2021. Geothermal analysis modeling and simulation using Idaho National Laboratory' RELAP5-3D-PRONGHORN coupled codes. Geotherm. Resour.Counc., Trans. 45, 53–67.

Parisi, C., Balestra, P., Kyanjo, B., Marshall, T.D., McLing, T.L., White, M.D., 2023. Closed loop geothermal analysis modeling and simulation using Idaho National Laboratory RELAP5-3D-FALCON coupled codes. In: Proceedings, 48th Workshop on Geothermal Reservoir Engineering Stanford University, Stanford, California, February 6–8, 2023. SGP-TR-224.

Podgorney, R.K., Finnila, A., Ghassemi, A., McLennan, J., Moore, J., 2020. Reference Native State and Stimulation Models of the Utah FORGE Site. In: Proceedings of the 45th Workshop on Geothermal Reservoir Engineering. Stanford University, Stanford, California. February 10-12, 2020, SGP-TR-216.

Podgorney, R., Finnila, A., Simmons, S., McLennan, J., 2021. A reference thermal-hydrologic-mechanical native state model of the Utah FORGE enhanced geothermal site. Energies 14 (16), 4758. https://doi.org/10.3390/en141664758.

Pruess, K., Oldenburg, C.M., Moridis, G.J., 2012. TOUGH2 User's Guide Version 2. Lawrence Berkeley National Laboratory, Berkeley, California. LBNL-43134 (revised).

Ramey, H.J., 1962. Wellbore heat transmission. Trans. Soc. Pet. Eng. 225 (4), 427–435. SPE-00811696.

RELAP5-3D Code Development Team, 2018a. RELAP5-3D Code Manual Volume I: Code Structure, System Models and Solution Methods. Idaho National Laboratory, Idaho Falls, Idaho. INL/MIS-15-36723, rev. 4.4.

RELAP5-3D Code Development Team, 2018b. RELAP5-3D Code Manual Volume IV: Models and Correlations. Idaho National Laboratory, Idaho Falls, Idaho. INL/MIS-15-36723, rev. 4.4.

Rennert, K., Errickson, F., Prest, B.C., Rennels, L., Newell, R.G., Pizer, W., Kingdon, C., Wingenroth, J., Cooke, R., Parthum, B., Smith, D., Cromar, K., Diaz, D., Moore, F., Müller, U.K., Plevin, R.J., Raftery, A.E., Ševčíková, H., Sheets, H., Stock, J.H., Tan, T., Watson, M., Wong, T.E., Anthoff, D., 2022. Comprehensive evidence implies a higher social cost of CO_2. Nature 610, 687–692. https://doi.org/10.1038/s41586-022-05224-9.

Robertson, E.C., 1988. *Thermal properties of rocks*, United States Department of the Interior Geological Survey, Reston, Virginia, Open-File Report 88-441.

Schulz, S.-U., 2008. "Investigations on the improvement of the energy output of a closed loop geothermal system (CLGS)," Dr.-Ing. Thesis, Technische Univ. Berlin (Germany). Fakultaet VI - Planen Bauen Umwelt, ETDE-DE-2106, OSTI ID: 21240869.

Sierra Thermal Fluid Development Team, 2020. SIERRA Multimechanics Module: Aria User Manual—Version 4.56. Sandia National Laboratories, Albuquerque, New Mexico. https://doi.org/10.2172/1615880. SAND-2020-4000 685399.

Song, X., Shi, Y., Li, G., Shen, Z., Hu, X., Lyu, Z., Zheng, R., Wang, G., 2018a. Numerical analysis of the heat production performance of a closed loop geothermal system. Renew. Energy 120, 365–378.

Song, X., Wang, G., Shi, Y., Li, R., Xu, Z., Zheng, R., Wang, Y., Li, J., 2018b. Numerical analysis of heat extraction performance of a deep coaxial borehole heat exchanger geothermal system. Energy 164, 1298–1310.

Sun, F., Yao, Y., Li, G., Li, X., 2018. Geothermal energy development by circulating CO_2 in a U-shaped closed loop geothermal system. Energy Convers. Manag. 174, 971–982.

Tester, J.W., Anderson, B., Batchelor, A., Blackwell, D., DiPippo, R., Drake, E., Garnish, J., Livesay, B., Moore, M.C., Nichols, K., Petty, S., Toksoz, N., Veatch, R., Augustine, C., Baria, R., Murphy, E., Negraru, P., Richards, M., 2006. The Future of Geothermal Energy: Impact of Enhanced Geothermal Systems (EGS) On the United States in the 21st Century. Massachusetts Institute of Technology, Cambridge, Massachusetts. DOE Contract DE-AC07-05ID14517, Final Report.

Vasyliv, Y., Bran-Anleu, G.A., Kucala, A., Subia, S., Martinez, M., 2021. Analysis and optimization of a closed loop geothermal system in hot rock reservoirs. Geotherm. Resour.Counc., Trans. 45, 116–131.

Wang, G., Song, X., Shi, Y., Yulong, F., Yang, R., Li, J., 2020. Comparison of production characteristics of various coaxial closed-loop geothermal systems. Energy Convers. Manag. 225. https://doi.org/10.1016/j.enconman.2020.113437.

Wang, G., Song, X., Shi, Y., Yang, R., Yulong, F., Zheng, R., Li, J., 2021. Heat extraction analysis of a novel multilateral-well coaxial closed-loop geothermal system. Renew. Energy 163, 974–986.

Wang, X., Pan, C., Romero, C.E., Qiao, Z., Banerjee, A., Rubio-Maya, C., Pan, L., 2022. Thermo-economic analysis of a direct supercritical CO_2 electric power generation system using geothermal heat. Front. Energy 16 (2), 246–262.

White, M.D., Bacon, D.H., White, S.K., Zhang, Z.F., 2013. Fully coupled well models for fluid injection and production. Energy Procedia 37, 3960–3970. https://doi.org/10.1016/j.egypro.2013.06.295.

White, M.D., Fu, P., 2020. Application of an embedded fracture and borehole modeling approach to the understanding of EGS collab experiment 1. In: Proceedings, 45th Workshop on Geothermal Reservoir Engineering, Stanford University, Stanford, California, February 10–12, 2020. SGP-TR-216.

White, M.D., Martinez, M., Vasyliv, Y., Bran-Anleu, G.A., Parisi, C., Balestra, P., Horne, R. N., Augustine, C., Pauley, L., Hollett, D., Bettin, G., Marshall, T., Group, C.L.W., 2021. Thermal and mechanical energy performance analysis of closed-loop systems in hot-dry-rock and hot-wet-rock reservoirs. Geotherm. Resour.Counc., Trans. 45, 132–149.

Zhang, W., Li, W., Sørensen, B.R., Cui, P., Man, Y., Yu, M., Fang, Z., 2021. Comparative analysis of heat transfer performance of coaxial pipe and U-type deep borehole heat exchangers. Geothermics 96. https://doi.org/10.1016/j.geothermics.2021.102220.